Frontiers of fracture and fatigue: Some recent applications of the local strain energy density

F. Berto, S.M.J. Razavi, J. Torgersen
Department of Mechanical and Industrial Engineering, Norwegian University of Science and Technology (NTNU), Norway
filippo.berto@ntnu.no, javad.razavi@ntnu.no, jan.torgersen@ntnu.no

ABSTRACT. The phenomenon of brittle fracture occurs too often in various branches of engineering being the reason of unexpected termination of anticipated service lives of an engineering objects. This leads to unfortunate catastrophic structural failures resulting in loss of lives and in excessive costs. The theory of fracture mechanics enables the analysis of brittle and fatigue fracture and helps to prevent the occurrence of brittle failure. This field has engaged researchers from various fields of engineering from the early days until today. As its own scientific discipline, it is now less than fifty years old and encourages scientists and engineers to speak the same language when dealing with the design and manufacturing of the classical machinery as well as various intricate devices of nanometer scale, or even smaller, reasoning significant scale effects that arise. Attempting to strike a common ground will connect various physical events/phenomena as a natural result of curiosity arising in course of joint research activities. The interpretation provided by the strain energy density to face different problems and applications is presented in this paper considering some recent outcomes at different scale levels.

KEYWORDS. Strain Energy Density; Control radius; Finite size volume; multiscale; Additive materials.

Citation: Berto, F., Razavi, S. M. J., Torgersen, J., Frontiers of fracture and fatigue: Some recent applications of the local strain energy density, Frattura ed Integrità Strutturale, 43 (2018) 1-32.

Received: 27.09.2017
Accepted: 30.10.2017
Published: 01.01.2018

Copyright: © 2018 This is an open access article under the terms of the CC-BY 4.0, which permits unrestricted use, distribution, and reproduction in any medium, provided the original author and source are credited.

INTRODUCTION

The phenomenon of brittle fracture is encountered in many aspects of everyday life and many catastrophic structural failures involving loss of life have occurred as a result of sudden, unexpected failure. The field of fracture mechanics and the fatigue behavior of structural materials is focused on the prevention of brittle fracture and, as a scientific discipline in its own right, is less than fifty years old. However, the concern over brittle fracture is not new and the origin of the design to ensure safety of structures against sudden collapse is very old. This topic has involved many researchers in different engineering fields from ancient time to nowadays. Materials may fail at different scale levels with some similarities in the final behavior but also with strong scale effects characterizing the different scales of observation.

A powerful parameter able to fully include the scale effect is the local strain energy density as recently discussed by Sih and co-authors in Refs [1-6]. Taking into account recent advances regarding new materials as well as those developed for aggressive environments or obtained by additive manufacturing processes, the present paper is aimed to give a complete overview of the volume based strain energy density approach [7-16].

The concept of "elementary" volume was first used many years ago by Neuber [17-19] and it states that not the theoretical maximum notch stress is the static or fatigue strength-effective parameter in the case of pointed notches, but rather the notch stress averaged over a short distance normal to the notch edge. In high cycle fatigue regime, the integration path should coincide with the early fatigue crack propagation path. A further idea was to determine the fatigue-effective notch stress directly (i.e. without notch stress averaging) by performing the notch stress analysis with a fictitiously enlarged notch radius, ϱ_f, corresponding to the relevant support [20-26].

Fundamentals of Critical Distance Mechanics applied to static failure have been developed in [27, 28]. This "Point Criterion" becomes a "Line criterion" in Refs. [29-31] who dealt with components weakened by sharp V-shaped notches. Afterwards, this critical distance-based criterion was extended also to structural elements under multi-axial loading [32, 33] by introducing a non-local failure function combining normal and shear stress components. The pioneering work by Sheppard has to be mention at this point. In fact dealing with notched components the idea that a quantity averaged over a finite size volume controls the stress state in the volume by means of a single parameter, has been first introduced in [34].

For many years the Strain Energy Density (SED) has been used to formulate failure criteria for materials exhibiting both ductile and brittle behavior. Since Beltrami [35] to nowadays the SED has been found being a powerful tool to assess the static and fatigue behavior of notched and unnotched components in structural engineering. Different SED-based approaches were formulated by many researchers.

Dealing here with the strain energy density concept, it is worthwhile contemplating some fundamental contributions by Sih [36-40]. The strain energy density factor S was defined as the product of the strain energy density by a critical distance from the point of singularity. Failure was thought of as controlled by a critical value S_c, whereas the direction of crack propagation was determined by imposing a minimum condition on S.

The deformation energy required for crack initiation in a unit volume of material is called Absorbed Specific Fracture Energy (ASFE) and its links with the critical value of J_c and the critical factor S_c were widely discussed. This topic was deeply considered in Refs. [41-44]. The concept of strain energy density has also been reported in the literature in order to predict the fatigue behavior of notches both under uniaxial and multi-axial stresses [45-46].

It should be remembered that in referring to small-scale yielding, a method based on the averaged of the stress and strain product within the elastic-plastic domain around the notch was extended to cyclic loading of notched components [47]. In particular in Ref. [48] it was proposed a *fatigue master life curve* based on the use of the plastic strain energy per cycle as evaluated from the cyclic *hysteresis loop* and the positive part of the elastic strain energy density.

The averaged strain energy density criterion, proposed in Refs [7-16], states that brittle failure occurs when the mean value of the strain energy density over a control volume (which becomes an area in two dimensional cases) is equal to a critical energy W_c. The SED approach is based both on a precise definition of the control volume and the fact that the critical energy does not depend on the notch sharpness. The control radius R_0 of the volume, over which the energy has to be averaged, depends on the ultimate tensile strength, the fracture toughness and Poisson's ratio in the case of static loads, whereas it depends on the unnotched specimen's fatigue limit, the threshold stress intensity factor range and the Poisson's ratio under high cycle fatigue loads.

Several criteria have been proposed to predict fracture loads of components with *notches*, subjected to *mode I loading* [49-65]. The problem of brittle failure from *blunted notches* loaded under *mixed mode* is more complex than in mode I loading and experimental data, particularly for notches with a non- negligible radius, has been faced by other criteria [66-69] and only recently with the SED approach [70-76].

In the recent years the SED has been applied to assess the fracture behavior of innovative materials subjected to aggressive environmental conditions as well as to micro-components and additive manufactured materials showing some sound advantages that will be discussed in more details in the present contribution. In particular after this short introduction the analytical background of the SED approach will be discussed in section 2. Master curves for static and fatigue loadings obtained reanalyzing more than 2000 data taken from the literature will be presented in section 3 while in section 4 the advantages of the approach will be discussed considering in particular the capacity of taking into account 3d effects and the capacity of the criterion to take into account in an unified way internal defects of the material and geometrical discontinuities. In section 5 some recent applications will be discussed considering materials subjected to multiaxial loadings and high temperature. Some advanced applications related to fracture at nano-scale, fatigue behavior of additive manufactured materials and new generations of welding techniques will be treated.

ANALYTICAL BACKGROUND OF THE STRAIN ENERGY DENSITY APPROACH

The SED approach is based on the idea that under tensile stresses failure occurs when $\bar{W} = W_c$, where the critical value W_c obviously varies from material to material. If the material behaviour is ideally brittle, then W_c can be evaluated by using simply the conventional ultimate tensile strength σ_t, so that $W_c = \sigma_t^2 / 2E$.

In plane problems, the control volume becomes a circle or a circular sector with a radius R_0 in the case of cracks or pointed V-notches in mode I or mixed, I+II, mode loading (Fig. 1a,b). Under plane strain conditions, a useful expression for R_0 has been provided considering the crack case [49]:

$$R_0 = \frac{(1+\nu)(5-8\nu)}{4\pi}\left(\frac{K_{IC}}{\sigma_t}\right)^2 \tag{1}$$

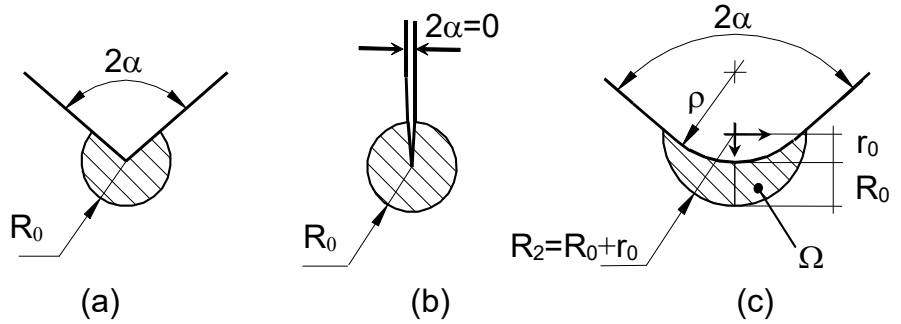

Figure 1: Critical volume (area) for sharp V-notch (a), crack (b) and blunt V-notch (c) under mode I loading.

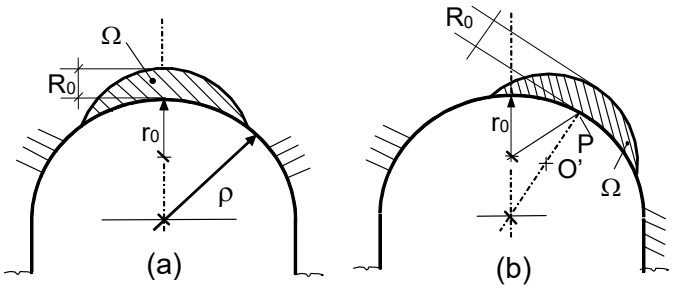

Figure 2: Critical volume for U-notch under mode I (a) and mixed mode loading (b). Distance $r_0=\varrho/2$ [49].

In the case of blunt notches, the area assumes a crescent shape, with R_0 being its maximum width as measured along the notch bisector line (Fig. 1c) [70, 71]. Under mixed-mode loading, the control area is no longer centered with respect to the notch bisector, but rigidly rotated with respect to it and centered on the point where the maximum principal stress reaches its maximum value [70, 71]. This rotation is shown in Fig. 2 where the control area is drawn for a U-shaped notch both under mode I loading (Fig.2a) and mixed-mode loading (Fig. 2b).

It is possible to determine the total strain energy over the area of radius R_0 and then the mean value of the elastic SED referred to the area Ω. The final relationship is

$$\bar{W}_1 = \frac{I_1}{4\,E\,\lambda_1\,(\pi-\alpha)}\left(\frac{K_1}{R_0^{1-\lambda_1}}\right)^2 \tag{2}$$

where λ_1 is Williams' eigenvalue [77] and K_1 the mode I notch stress intensity factor. The parameter I_1 is different under plane stress and plane strain conditions [7].

In the presence of rounded V-notches it is possible to determine the total strain energy over the area Ω and then the mean value of the SED. When the area embraces the semicircular edge of the notch (and not its rectilinear flanks), the mean

value of SED can be expressed in the following form [11]

$$\overline{W}_1^{(e)} = \frac{E_1^{(e)}}{\Omega} = F(2\alpha)\ H(2\alpha, \frac{R_0}{\rho})\ \frac{\sigma^2{}_{\max}}{E} \tag{3}$$

where F(2α) depend on previously defined parameters
H is summarised in Refs [11, 15-16] as a function of opening angles and Poisson's ratios.
Under mixed mode loading the problem becomes more complex than under mode I loading, mainly because the maximum elastic stress is out of the notch bisector line and its position varies as a function of mode I to mode II stress distributions. The problem was widely discussed considering different combination of mode mixity [70, 71].
The expression for U-notches under mixed mode is analogous to that valid for notches in mode I:

$$\overline{W}^{(e)} = H^*\left(2\alpha, \frac{R_0}{\rho}\right) \times \frac{\pi\sigma_{\max}^2}{4E} \tag{4}$$

where $\sigma_{\max}$ is the maximum value of the principal stress along the notch edge and H^* depends again on the normalised radius R/R_0, the Poisson's ratio ν and the loading conditions. For different configurations of mode mixity, the function H, analytically obtained under mode I loading, was shown to be very close to H^*. This idea of equivalent local mode I was discussed in previous works [70-73].

MASTER CURVES FOR STATIC AND FATIGUE LOADINGS

Dealing with static loading a large bulk of data taken from the literature have been summarized in a single master curve.
The local SED values have been normalized to the critical SED values (as determined from unnotched specimens) and plotted as a function of the ϱ/R_0 ratio. The final synthesis has been carried out by normalizing the local SED to the critical SED values (as determined from unnotched, plain specimens) and plotting this non-dimensional parameter as a function of the ϱ/R_0 ratio. A scatterband is obtained whose mean value does not depend on ϱ/R_0, whereas the ratio between the upper and the lower limits are found to be about equal to 1.3/0.8=1.6 (Fig. 3). The strong variability of the non-dimensional radius ϱ/R_0 (notch root radius to control volume radius ratio, ranging here from about zero to about 500) makes stringent the check of the approach based on the local SED. The complete scatterband presented here (Fig. 3) has been obtained by updating the database containing failure data from 20 different ceramics, 4 PVC foams and some metallic materials [15, 16].
Dealing with the fatigue assessment of welded joints a scatterband has been proposed by Lazzarin and collaborators [7-10]. The mean value of the strain energy density (SED) in a circular sector of radius R_0 located at the fatigue crack initiation sites has been used to summarise fatigue strength data from steel welded joints of complex geometry (Fig. 4). The evaluation of the local strain energy density needs precise information about the control volume size. From a theoretical point of view the material properties in the vicinity of the weld toes and the weld roots depend on a number of parameters as residual stresses and distortions, heterogeneous metallurgical micro-structures, weld thermal cycles, heat source characteristics, load histories and so on. To device a model capable of predicting R_0 and fatigue life of welded components on the basis of all these parameters is really a task too complex. Thus, the spirit of the approach is to give a simplified method able to summarise the fatigue life of components only on the basis of geometrical information, treating all the other effects only in statistical terms, with reference to a well-defined group of welded materials and, for the time being, to arc welding processes.
The material parameter R_0 has been estimated by using the fatigue strength $\Delta\sigma_A$ of the butt ground welded joints (in order to quantify the influence of the welding process, in the absence of any stress concentration effect) and the NSIF-based fatigue strength of welded joints having a V-notch angle at the weld toe constant and large enough to ensure the non-singularity of mode II stress distributions.
A convenient expression is [7, 10]:

$$R_0 = \left(\frac{\sqrt{2e_1}\ \Delta K_{1A}^N}{\Delta\sigma_A}\right)^{\frac{1}{1-\lambda_1}} \tag{5}$$

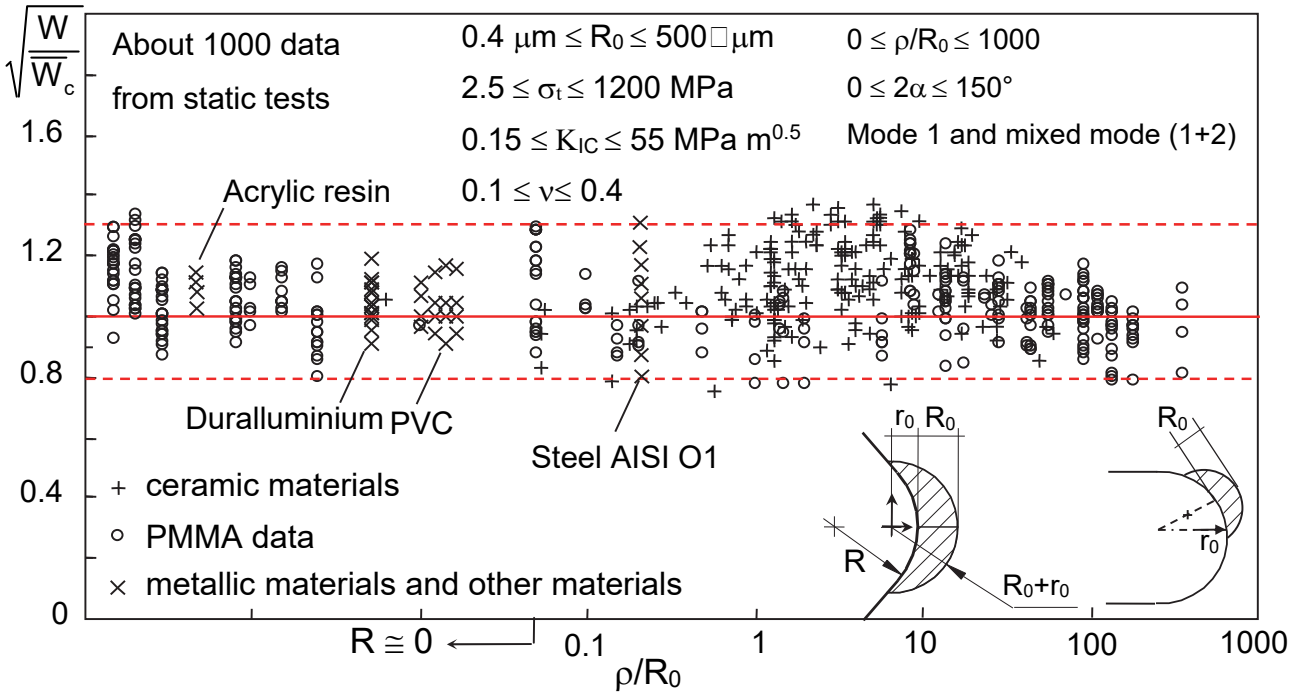

Figure 3: Synthesis of data taken from the literature. Different materials are summarized, among the others AISI O1 and duralluminium.

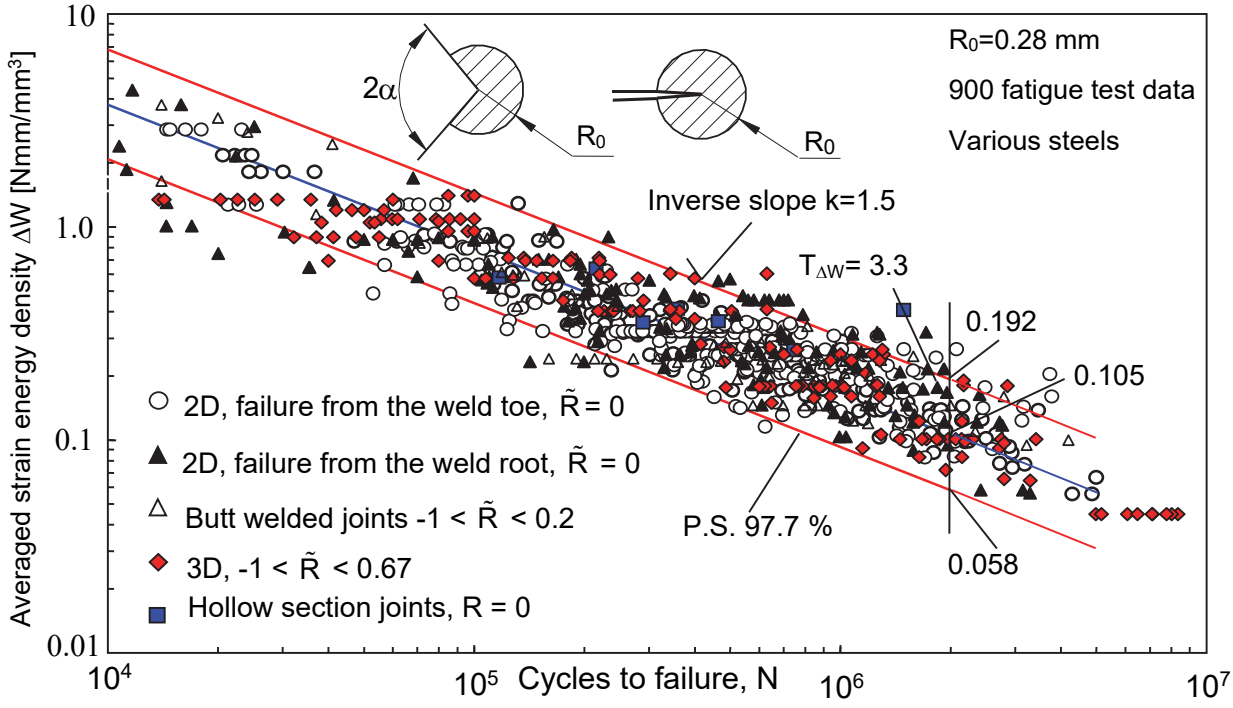

Figure 4: Fatigue strength of welded joints as a function of the averaged local strain energy density; R is the nominal load ratio.

where both λ_1 and e_1 depend on the V-notch angle. Eq. (5) makes it possible to estimate the R_0 value as soon as ΔK_{1A}^N and $\Delta\sigma_A$ are known. At $N_A = 5 \cdot 10^6$ cycles and in the presence of a nominal load ratio equal to zero a mean value ΔK_{1A}^N

equal to 211 MPa mm$^{0.326}$ was found re-analyzing experimental results taking from the literature [10, 15-16]. For butt ground welds made of ferritic steels a mean value $\Delta\sigma_A$ = 155 MPa (at N_A= 5·10^6 cycles, with R=0) was employed for setting the method. Then, by introducing the above mentioned value into Eq. (5), one obtains for steel welded joints with failures from the weld toe R_0 =0.28 mm.

By modelling the weld toe regions as sharp V-notches and using the local strain energy, more than 900 fatigue strength data from welded joints with weld toe and weld root failures were analyzed and the theoretical scatter band in terms of SED was obtained and recently updated with all the possible data available in the literature for which the local geometries were properly defined [16]. The geometry exhibited a strong variability of the main plate thickness (from 6 to 100 mm), the transverse plate (from 3 to 200 mm) and the bead flank (from 0 to 150 degrees). The synthesis of all those data is shown in Fig. 4, where the number of cycles to failure is given as a function of $\Delta\overline{W}_1$ (the Mode II stress distribution being non-singular for all those geometries). The figure includes data obtained both under tension and bending loads, as well as from "as-welded" and "stress-relieved" joints. The scatter index T_W, related to the two curves with probabilities of survival P_S= 2.3% and 97.7%, is 3.3, to be compared with the variation of the strain energy density range, from about 4.0 to about 0.1 MJ/m^3. T_W=3.3 becomes equal to 1.50 when reconverted to an equivalent local stress range with probabilities of survival P_S=10% and 90% ($T_W = \sqrt{3.3}\,/\,1.21 = 1.5$). The final synthesis based on more than 900 experimental data is shown in Fig. 4 where some recent results from butt welded joints, three-dimensional models and hollow section joints have been included. A good agreement is found, giving a sound, robust basis to the approach when the welded plate thickness is equal to or greater than 6 mm.

ADVANTAGES OF THE METHOD

As opposed to the direct evaluation of the stress intensity factors (SIFs) or generalized notch stress intensity factors (NSIFs), which need very refined meshes, the mean value of the elastic SED on the control volume can be determined with high accuracy by using coarse meshes [78-81]. Very refined meshes are necessary to directly determine the NSIFs from the local stress distributions. Refined meshes are not necessary when the aim of the finite element analysis is to determine the mean value of the local strain energy density on a control volume surrounding the points of stress singularity. The SED in fact can be derived directly from nodal displacements, so that also coarse meshes are able to give sufficiently accurate values for it. Some recent contributions document the weak variability of the SED as determined from very refined meshes and coarse meshes, considering some typical welded joint geometries and provide a theoretical justification to the weak dependence exhibited by the mean value of the local SED when evaluated over a control volume centered at the weld root or the weld toe. On the contrary singular stress distributions are strongly mesh dependent. The NSIFs can be estimated from the local SED value of pointed V-notches in plates subjected to mode I, Mode II or a mixed mode loading. Taking advantage of some closed-form relationships linking the local stress distributions ahead of the notch to the maximum elastic stresses at the notch tip the coarse mesh SED-based procedure is used to estimate the relevant theoretical stress concentration factor K_t for blunt notches considering, in particular, a circular hole and a U-shaped notch, the former in mode I loading, the latter also in mixed, I + II, mode [79, 80].

Other important advantages can be achieved by using the SED approach. The most important are as follows:

- It permits consideration of the scale effect which is fully included in the Notch Stress Intensity Factor Approach [15, 16]
- It permits consideration of the cycle nominal load ratio [15, 16].
- It overcomes the complex problem tied to the different NSIF units of measure in the case of different notch opening angles (i.e crack initiation at the toe (2α=135°) or root (2α =0°) in a welded joint) [10, 15-16]
- It overcomes the complex problem of multiple crack initiation and their interaction on different planes.
- It directly takes into account the T-stress and this aspect becomes fundamental when thin structures are analysed [82, 83].
- It permits consideration of the contribution of different Modes [70-76, 84-85].
- It directly includes three-dimensional effects and out-of-plane singularities not assessed by Williams' theory as it will be described in the next section.

Three-dimensional effects

Dealing with 3d effects the SED is able to take into account coupled induced modes pioneering investigated by Sih, Pook and Kotousov [86-93].

The problem considered here, as example, is a finite size plate containing a sharp V-notch, subjected to a remote shear stress. The geometry of the problem is shown in Fig. 5. The V-notch is characterized by a notch opening angle, 2*a* and a depth, a. The base and the height of the plate are 2*W* and *W*, respectively, while the plate thickness is 2*t*. To observe the dependence of the intensity and singular power of singular modes as a function of the notch angle, a range of finite element models are developed for notch angles of 2*a* = 45°, 60°, 90°, 102.6°, 120° and 135°. A typical example of the stress field through the thickness of the plate is shown in Fig. 6 at different distance from the notch tip [94-97].

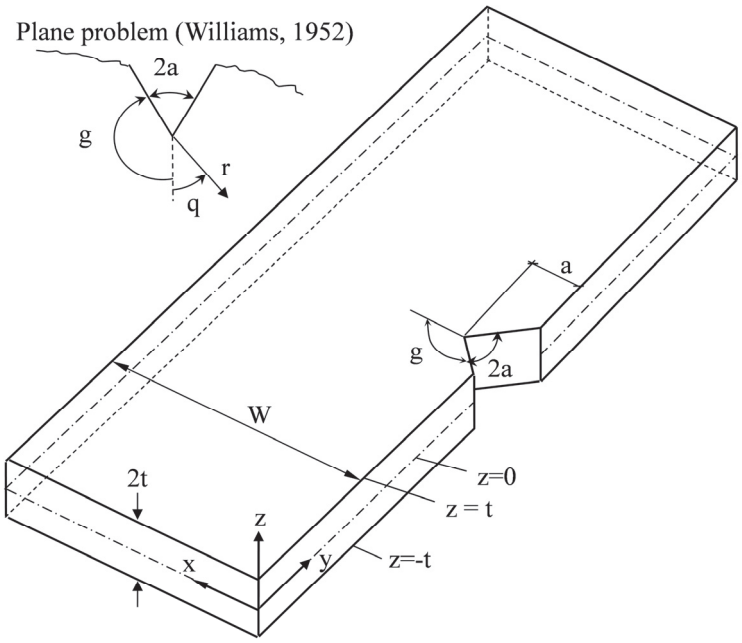

Figure 5: V-notch in a plane and in a three-dimensional plate.

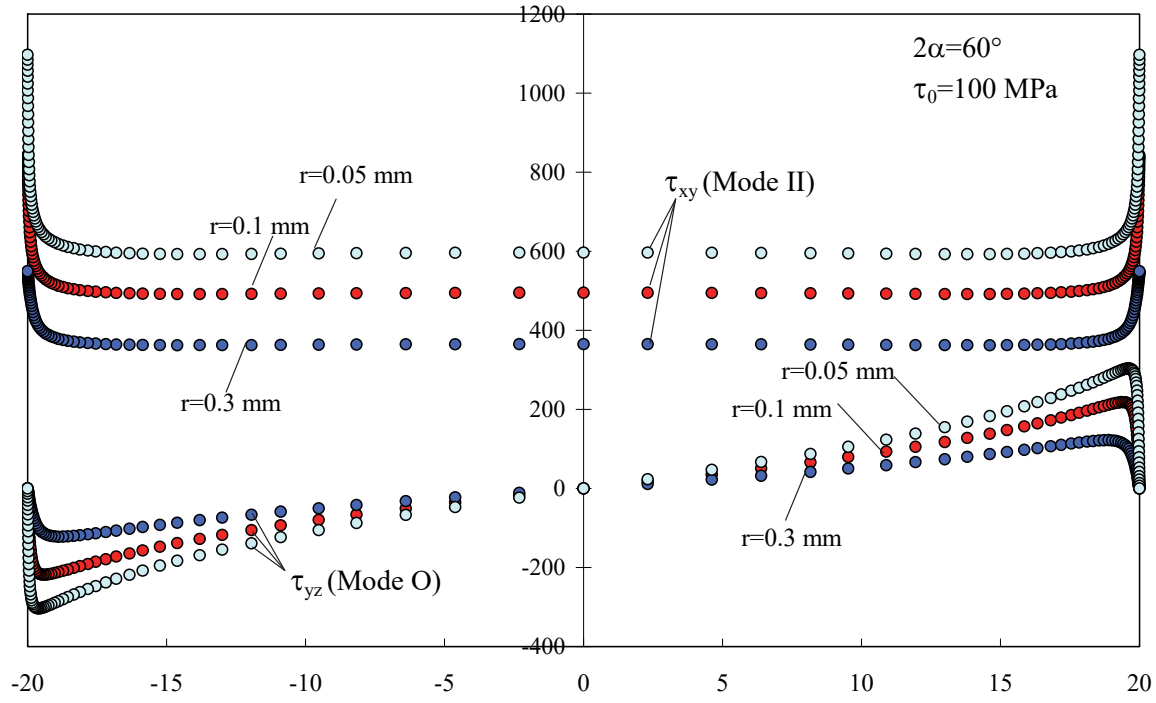

Figure 6: Mode II and mode O stress components plotted throughout the plate thickness (along the notch bisector line) at three different distances r from the point of singularity (*r*=*x*).

The stress fields of three plates scaled in a geometrical proportion are shown in Fig. 7. In these plates the notch opening angle is kept constant and equal to 90°. The geometrical parameters of the base geometry ($a = t = 20$ mm and $W = 200$ mm) are simultaneously multiplied or divided by a factor 100. The plots are drawn considering a plane at a distance of 2 mm from the surface for the base geometry ($z = 18$ mm). This distance is increased or reduced according to the scale factor (= 100) in the other two cases. The increase or decrease of the in-plane shear stress components is according to the scale factor of $(100)^{0.0915} = 1.52$. The variability of the out-of-plane shear stress components is much more pronounced, and according to the scale factor $(100)^{0.33} = 4.57$. The intersection point between τ_{yz} and τ_{yx} stress fields varies from case to case: this point is located at 1 mm from the V-notch tip when $a = 2000$ mm, at 10^{-2} mm when $a = 20$ mm and at 10^{-4} mm when $a = 0.20$ mm.

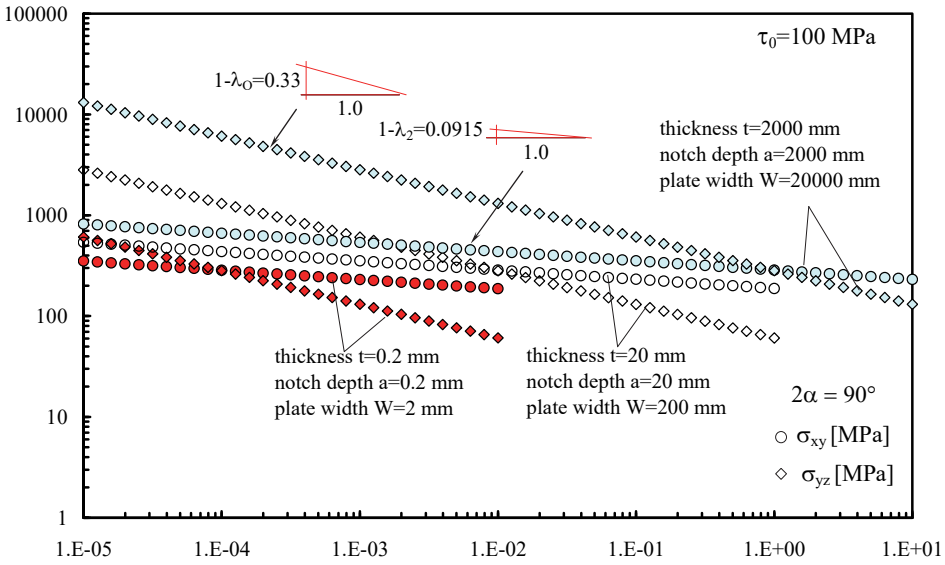

Figure 7: Mode O and mode II stress fields for three models scaled in geometrial proportion.

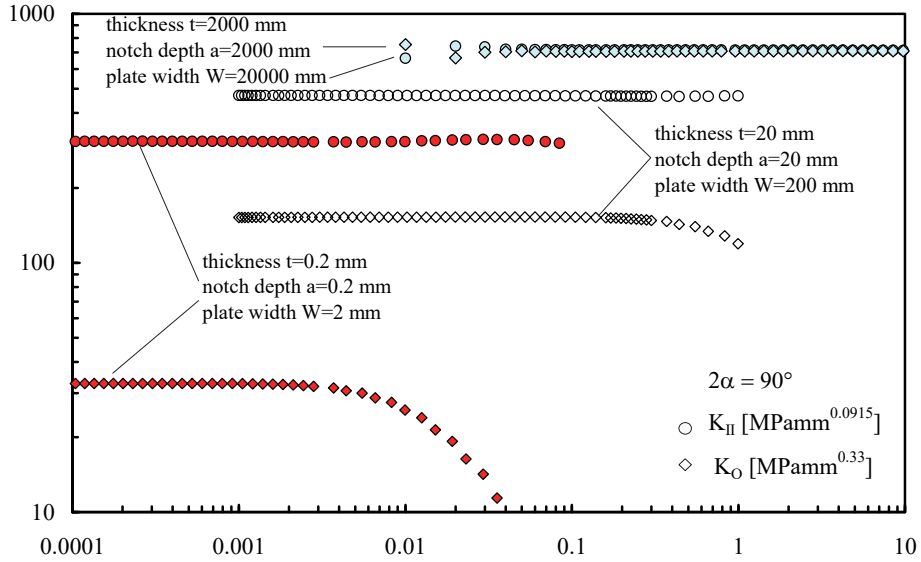

Figure 8: Notch stress intensità factors K_{II} and K_{O} for three plates scaled in geometrical proportion.

The plots of the corresponding notch stress intensity factors, K_O and K_{II}, are shown in Fig. 8. These factors are determined on the notch bisector line according to the following expressions

$$K_{II} = \sqrt{2\pi} \lim_{x \to 0} \tau_{yx} (x)^{1-\lambda_{II}} \tag{6}$$

$$K_{o} = \sqrt{2\pi} \lim_{x \to 0} \tau_{yz} (x)^{1-\lambda_{o}} \tag{7}$$

where K_{II} is according to the definition suggested by Gross and Mendelson [98], and K_O represents a natural extension of stress intensity factors for cracks.
The scale effect changes for 2α= 135° are due to the non-singular behavior of the in-plane shear stress, see Fig. 9. Once again, the base geometry is scaled in geometrical proportion, by multiplying all geometrical parameters by a factor 4 or by a factor 8. The mode O stress field increases with an increase of t whereas, on the contrary, the mode II stress field decreases with t.
Recently Pook and co-authors have analyzed the corner singularities showing the possibilities of taking into account of these effects by means of the strain energy density in cracked plates [99-100] confirming the same results obtained by using J-integral by He et al. [101].
Figs. 10 shows that through the thickness SED distributions, for t/a = 0.50, 1, 2 and 3, is able to take into account the through-the-thickness corner point singularities as a function of the ratio between the thickness of the plate and the crack length.
The results show that the change of loading mode from nominal mode III to nominal mode II has had no effect on the distributions of τ_{yz} and τ_{xy} on and near the crack surface, but has significantly changed the through thickness distributions of K_{II}, K_{III} (which are difficult to define close to the free surface of the plate) and the SED.

Capacity of treating material defects and geometrical discontinuity in a unified way

The SED approach is able to treat in a unified way internal defects and geometrical discontinuities and this is a very strong advantage dealing with additive manufactured materials.
As well discussed in [102] approach SED can be applied to components weakened by cracks/defects and blunt V-shaped notches. As a result, Kitagawa [103] and Atzori's diagrams [104-105] reported in the literature to summarize fatigue limit of cracked and notched components can be immediately derived, creating a natural transition between the Linear Elastic Fracture Mechanics and the Linear Notch Mechanics.
Consider a long crack in a plate subject to a remotely applied tensile stress. The mean value of the elastic strain energy referred to the area shown in Fig. 1.b is:

$$\bar{W}_1 = \frac{I_1}{2E} \frac{(K_I)^2}{\pi R_0} \tag{8}$$

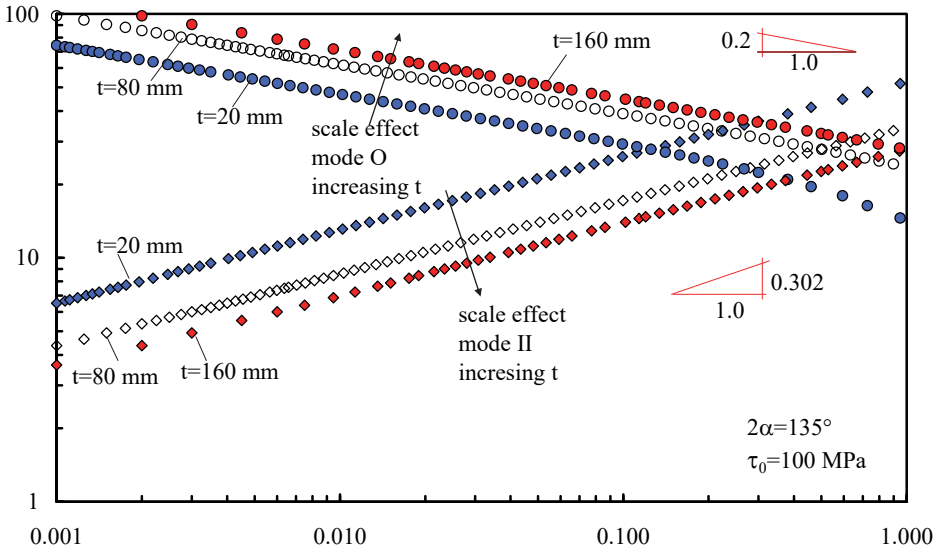

Figure 9: Mode O and mode II stress fields for three models scaled in geometrial proportion.

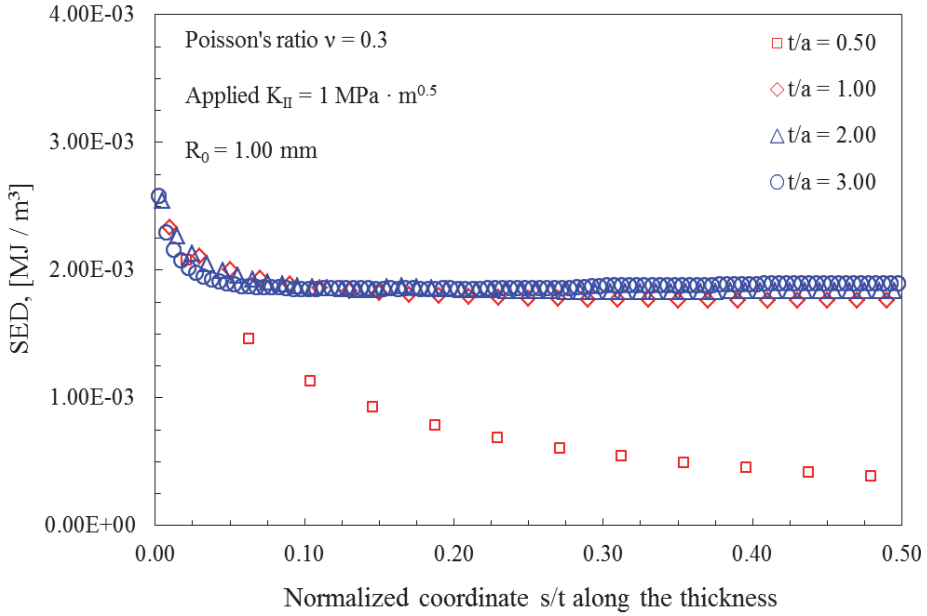

Figure 10: Through-the-thickness *SED* distribution for t/a = 0.50, 1, 2, 3. Control radius R_0 = 1.00 mm.

Some FE analyses were carried out under plane strain conditions by modelling cracks of different length in an infinite plate and using two values for the radius R_0, 0.02 mm and 0.2 mm, respectively. Elastic properties were kept constant, E= 206000 MPa and ν=0.3. The toughness is thought of as correlated to the inverse of the mean value of strain energy, $\overline{W}_1$. Fig. 11 plots $1/\overline{W}_1$ as a function of the crack amplitude a. The plateau on the left hand side of Fig. 2 is due to the fact that the small cracks are fully embedded in the elementary structural volume, so that the value of $\overline{W}_1$ coincides with that of the points far away from the crack, $\sigma_0^2(1-\nu^2)/(2E)$, where $(1-\nu^2)$ is due to plane strain conditions in the FE model.

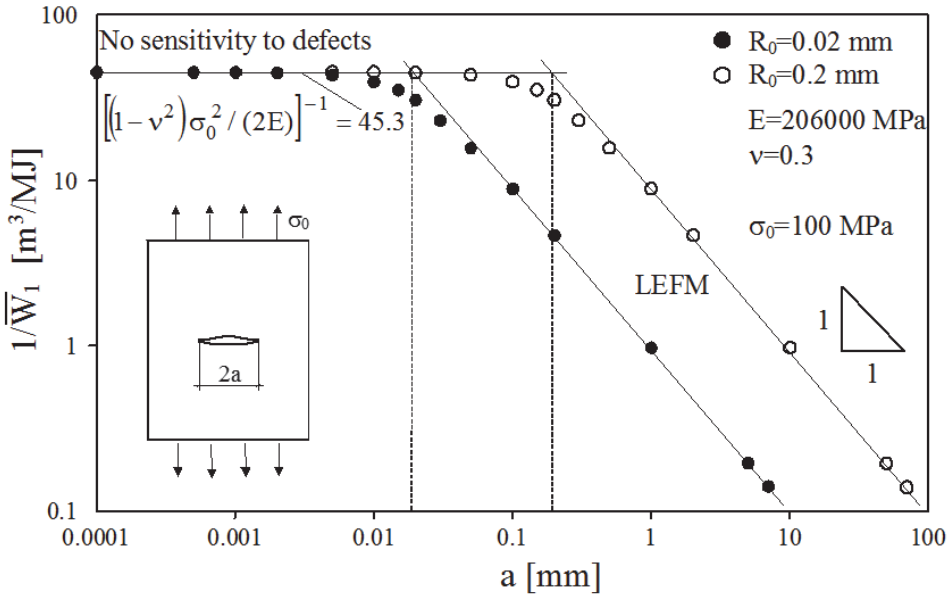

Figure 11: Influence of crack amplitude on finite-volume-energy (plane strain, infinite plate).

Under fatigue limit conditions we introduce ΔK_{th} and $\Delta\sigma_0$ into Eq.(1), where $\Delta\sigma_0$ is the plain specimen fatigue limit and ΔK_{th} the threshold value of the stress intensity factor range for long cracks under Mode I conditions. Now the critical radius becomes:

$$R_0 = \frac{(1+\nu)(5-8\nu)}{4\pi}\left(\frac{\Delta K_{th}}{\Delta\sigma_0}\right)^2 \tag{9}$$

When ν=0.3, Eq. (4) gives R_c=0.845a_0, where $a_0 = (1/\pi)(\Delta K_{th}/\Delta\sigma_0)^2$ is the El Haddad-Smith-Topper parameter [106]. Under plane stress conditions, simple algebraic considerations give:

$$R_0 = \frac{(5-3\nu)}{4\pi}\left(\frac{\Delta K_{th}}{\Delta\sigma_0}\right)^2 \tag{10}$$

so that we have now R_0=1.025a_0 when the Poisson's ratio ν is 0.3.
Fig. 11 exactly fits the Kitagawa diagram plotting fatigue strength of a material in the presence and absence of cracks [103]. The plateau on the left hand side of Fig. 2 is due to the fact that the small cracks are fully embedded in the elementary structural volume, so that the value of $\bar{W}_1$ coincides with that of the plain specimens (under plane strain conditions).
The transition crack size a_0 has been employed as an empirical parameter to account for the differences between long and short fatigue cracks. In particular El Haddad *et al.* [106] suggested to add in the SIF range definition the fictitious crack length a_0 to the crack amplitude a. Doing so, the fatigue limit $\Delta\sigma_{th}$ of cracked components was correlated to plain specimen fatigue limit by means of the expression:

$$\frac{\Delta\sigma_{th}}{\Delta\sigma_0} = \frac{1}{\sqrt{1+a/a_0}} \tag{11}$$

By observing Fig. 11, when $a>>R_0$, it is possible to write:

$$\frac{\bar{W}_1^{\mathrm{Re}\,f}}{\bar{W}_1(a)} = \frac{\bar{W}_1^{\mathrm{Re}\,f}}{\bar{W}_1^{\mathrm{Re}\,f}(1+aI_1/R_0)} = \frac{1}{1+aI_1/R_0} = \frac{1}{1+a/a_0} \tag{12}$$

where $\bar{W}_1^{\mathrm{Re}\,f} = \sigma_0^2/2E$ is the reference value. The analogy with Eq.(11) is evident.

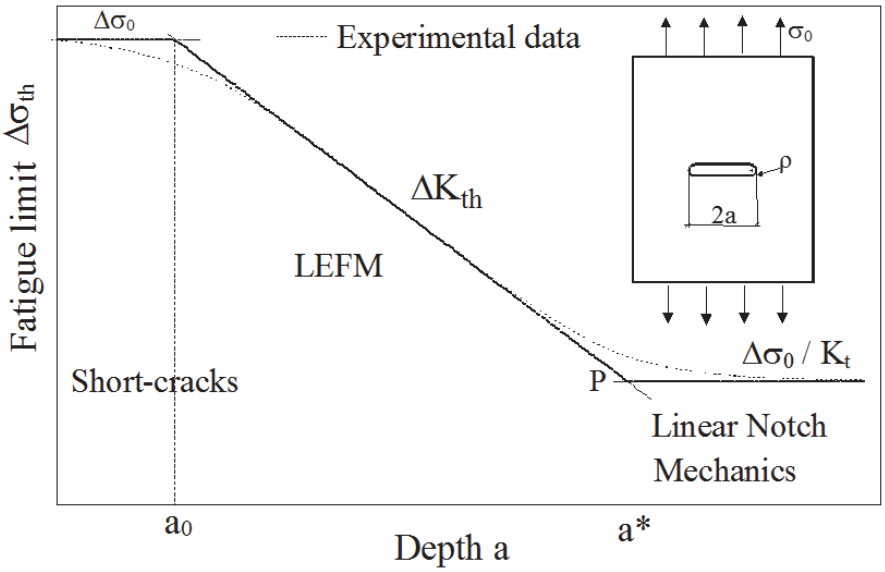

Figure 12: Fatigue behavior of a material weakened by notches or cracks (log-log scale).

The Kitagawa diagram was extended to blunt notches in 2001 [104] and then applied to summarize a number of experimental data taken from the literature [105]. The diagram was obtained by imposing the constancy of the notch acuity, a/ϱ, where a and ϱ are the notch semi-depth and the notch root radius, respectively. The constancy of that ratio results in the constancy of the theoretical stress concentration factor K_t. With respect to the crack case, there exists now a second plateau on the right hand side of the diagram. When the notch acuity is infinite, the diagram degenerates into the Kitagawa diagram, which appears to be a particular case of the diagram in [104]. Since it is valid the expression $a^* = K_t^2 a_0$, K_t and a_0 determine the position of point *P*, which is the ideal breaking point between LEFM and Linear Notch Mechanics. It is worth noting that the real behavior shown in Fig. 12 differs from the full a^*; the "sensitivity to defects" present in correspondence of a_0.

Consider again the elementary volume of material shown in Fig. 1-c. R_0 is measured along the notch bisector while the origin of the arc delimitating the volume is at a distance $\varrho/2$ from the notch tip. A number of FE analyses allowed us to determine the mean value of the strain energy over the volume. The results are plotted in Fig. 13, where the inverse of $\overline{W}_1$ is plotted against the notch depth a (or the notch root ϱ). It is evident that the constancy of R_0 is able to assure the presence of a double plateau and a natural transition between the three regions of the diagram.

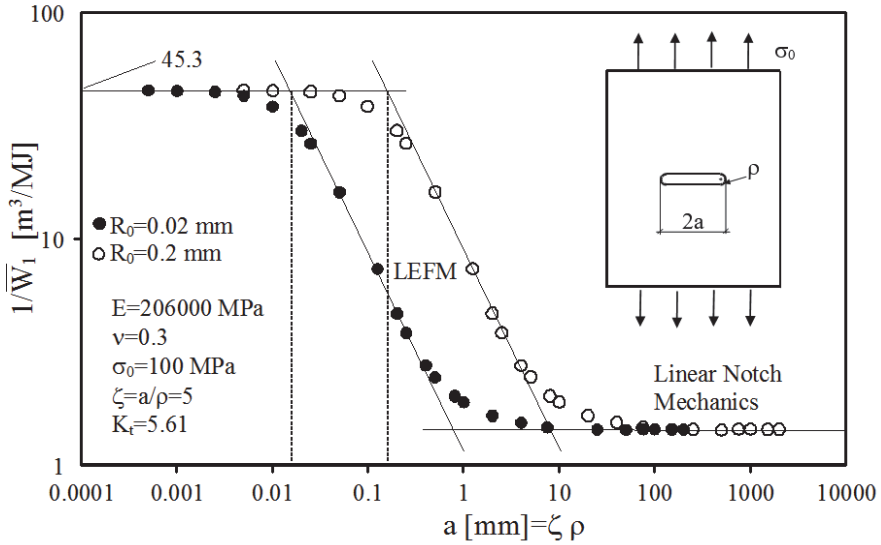

Figure 13: Influence of the notch depth on the finite-volume-energy (plane strain, infinite plate).

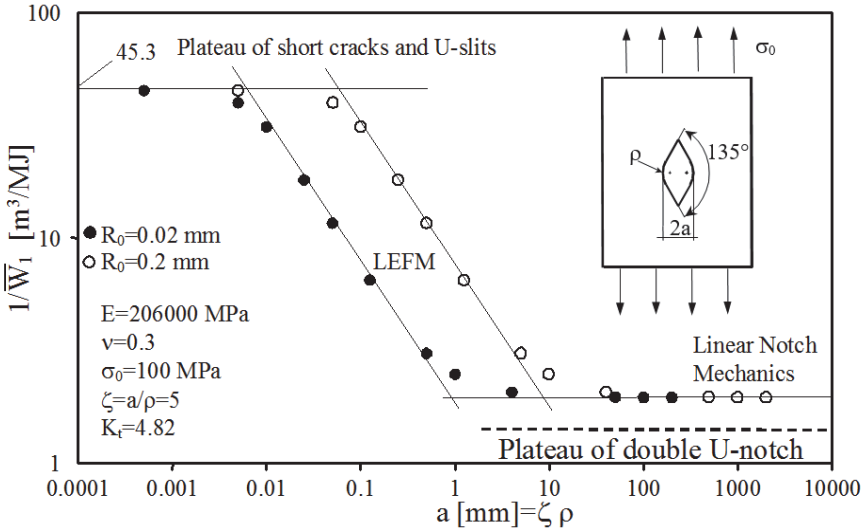

Figure 14: Influence of notch depth on finite-volume-energy (plane strain, infinite plate).

Finally, a variety of diamond-like notches were considered, all characterized by a notch angle of 135 degrees. R_0 is measured along the notch bisector, while the origin of the arc delimitating the volume is at a distance r_0 from the notch tip, being 0. The results are as shown in Fig. 14. On the left hand side, the plateau does not vary with respect to the crack and U-slit cases, while different is the intersection between the plateau and the LEFM line; on the right hand side of the diagram, the fatigue limit is greater than the double U-notch case, because of the reduction of the stress concentration factor K_t. The capacity of unifying notch mechanics and fracture mechanics in a single diagram by means of SED can be advantageously used for facing the structural integrity of complex components obtained by means of additive manufacturing processes.

APPLICATIONS

Multiaxial Fatigue

The strain energy density approach has been recently applied to complex multiaxial fatigue loadings [107-110]. In this section as example the last results dealing with the multiaxial fatigue strength of severely notched titanium grade 5 alloy (Ti-6Al-4V) is discussed [110]. Experimental tests under combined tension and torsion loading, both in-phase and out-of-phase, have been carried out on axisymmetric V-notched specimens considering different nominal load ratios (R = -1, 0, 0.5). All specimens were characterized by a notch tip radius less than 0.1 mm, a notch depth of 6 mm and a notch opening angle equal to 90 degrees. The diameter of the net transverse area is equal to 12 mm in all the specimens. The experimental data from multiaxial tests are compared with those from pure tension and pure torsion tests on un-notched and notched specimens, carried out at load ratio ranging from R = -3 to R=0.5.

In total over 160 new fatigue data are analyzed, first in terms of nominal stress amplitudes referred to the net area and then in terms of the local strain energy density averaged over a control volume surrounding the V-notch tip. The dependence of the control radius by the loading mode has been analyzed showing a very different notch sensitivity for tension and torsion. For the titanium alloy Ti-6Al-4V the control volume has been found to be strongly dependent on the loading mode [110]. It has been possible to estimate the control volume radii R_1 and R_3, considering separately the loading conditions of Mode I and Mode III. These radii are functions of the high cycle fatigue strength of smooth specimens, $\Delta\sigma_{1A}$ = 950 MPa, $\Delta\tau_{3A}$ = 776 MPa, and of the mean values of the NSIFS, ΔK_{1A} and ΔK_{3A}, all referred to the same number of cycles, $N_A = 2\times10^6$. In [110] it has been found as a result: R_1 = 0.051 mm and R_3 = 0.837 mm. The obtained values have been used to summarize all fatigue strength data by means of the averaged SED. The expressions for estimating the control radii, thought of as material properties, have been obtained imposing at N_A cycles the constancy of the SED from smooth and V-notched specimens, which depends on the notch stress intensity factors and the radius of the control volume. Considering instead cracked specimens, the critical NSIFs should be replaced by the threshold values of the stress intensity factors. In particular, a control volume of radius R_1 will be used to evaluate the averaged contribution to local stress and strains due to tensile loading, whereas a radius R_3 will be used to assess the averaged contribution due to torsion loading. The size of R_3 radius is highly influenced by the presence of larger plasticity under torsion loading with respect to tensile loading and by friction and rubbing between the crack surfaces, as discussed extensively for different materials [108]. With the aim to unify in a single diagram the fatigue data related to different values of the nominal load ratio R, it is necessary to introduce as made also above the weighting factor c_w on the basis of mere algebraic considerations. The result of these observations provides as master cases c_w = 1.0 for R = 0 and c_w = 0.5 for R = -1 [9].

Figs. 15 and 16 show the synthesis by means of local SED of all the experimental data from the fatigue tests at a nominal load ratio R = 0 and R = -1, respectively. The control radii have been found to be 0.051 mm and R_3 = 0.837 mm. The scatterbands have been defined considering the range 10-90% for the probability of survival. It can be observed that the inverse slope k equals 5.44 for R = 0 case and 5.25 for R = -1 case, while the corresponding values of the strain energy density at 2×10^6 cycles are 2.72 MJ/m^3 and 2.60 MJ/m^3. The SED-based scatter index T_W is 1.76 for R = 0 and 2.25 for R = -1 case, which would become equal to 1.33 and 1.50 respectively once reconverted *a posteriori* into equivalent stress-based scatter indexes T_W, by simply making the square root of the SED values. The values of the equivalent scatter index are satisfactory for engineering strength assessment, considering that each synthesis is performed on fatigue data from un-notched and V-notched specimens under pure tension, pure torsion or combined tension-torsion loading, both in phase and out-of-phase. Figs. 17 and 18 show instead the synthesis by means of average SED of all the experimental data from the fatigue tests of un-notched and V-notched specimens, respectively. Also in this case two control radii equal to R_1 = 0.051 mm and R_3 = 0.837 mm respectively have been used. It can be observed that the inverse slope k of the scatterbands equals 6.54 for un-notched specimens and 5.86 for V-notched ones, while the values of the strain energy density at 2×10^6 cycles are equal to 3.34 MJ/m^3 and 3.09 MJ/m^3, respectively. In this case T_W equals 2.50 for un-notched specimens and

2.20 for V-notched ones, which would give 1.58 and 1.48 respectively once reconverted *a posteriori* into equivalent stress-based scatter indexes T_σ. Also in this case the values of the scatter index are very satisfactory, given that the synthesis are based on fatigue data respectively from un-notched specimens under pure tension and torsion with different values of the load ratio and from V-notched specimens under pure tension, pure torsion or combined tension-torsion loading, with different values both of the load ratio and the phase angle. Finally in Fig. 19 the synthesis in terms of SED of all the fatigue strength data presented in this contribution is shown. Again two different control radii equal to R_1 = 0.051 mm and R_3 = 0.837 mm respectively have been adopted. The scatterband includes all the data from un-notched and V-notched specimens under pure tension, pure torsion and multiaxial loading, regardless of the load ratio and the phase angle. It is also characterized by an inverse slope k equal to 5.90, a scatter index T_W = 2.5 and a value of the strain energy density at the reference number of cycles, $N_A = 2\times10^6$, that equals 3.08 MJ/m³. The equivalent stress-based scatter index T_σ results to be 1.58, that is comparable with that observed in the Haibach scatterband (T_σ= 1.50). From Fig. 20 the unifying capacity of the SED approach can be easily observed, in fact it is capable of synthesize all the fatigue strength data in a single quite-narrow scatterband regardless of the loading mode and the specimens geometry.

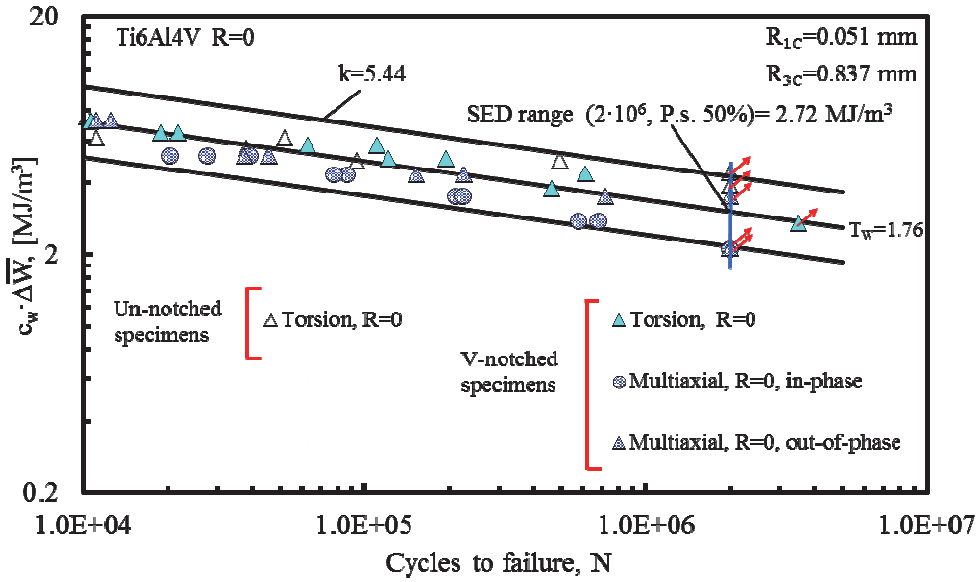

Figure 15: Synthesis by means of local SED of series data with R = 0.

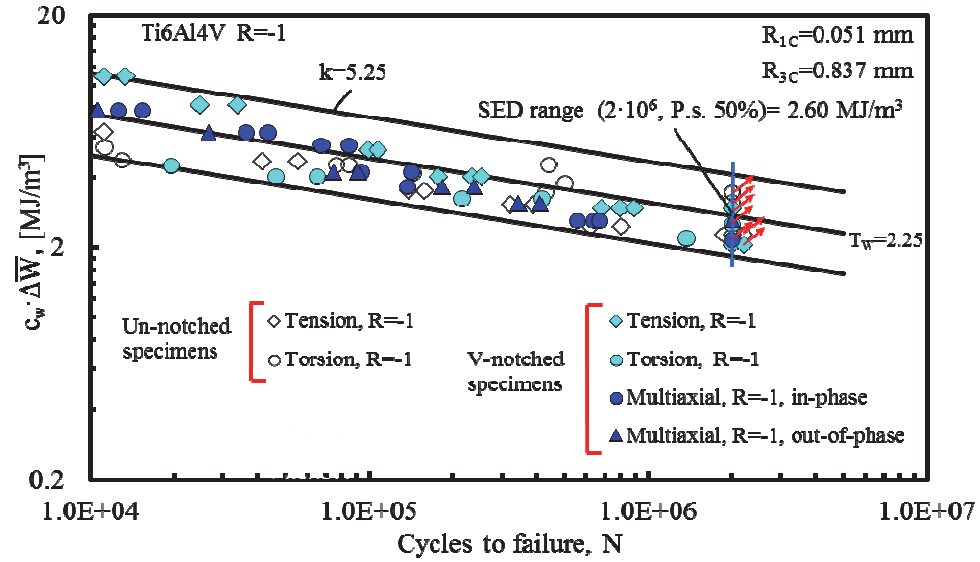

Figure 16: Synthesis by means of local SED of series data with R = -1.

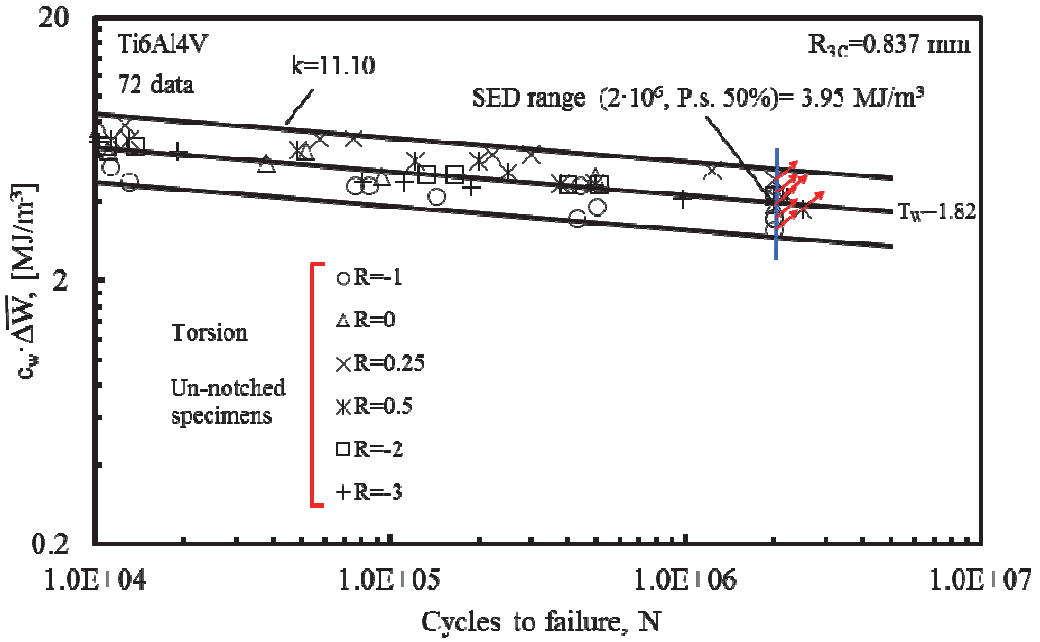

Figure 17: Synthesis by means of local SED of un-notched specimens' data under pure torsion.

Fatigue at high temperature

In recent years, the interest on fatigue assessment of steels and different alloys at high temperature has increased continuously [111-121]. In fact, high-temperature applications have become ever more important in different engineering fields, e.g. turbine blades of jet engine, nuclear power plant, molds for the continuous casting of steel, hot rolling of metals. In parallel, in order to bear mechanical loadings combined with critical conditions at high temperature, the development and testing of innovative materials has progressed substantially [122]. Among the traditional alloys available for this kind of applications, Cu-Be alloys surely stand out and fall within the most interesting materials suitable not only for high-temperature applications (Fig. 20).

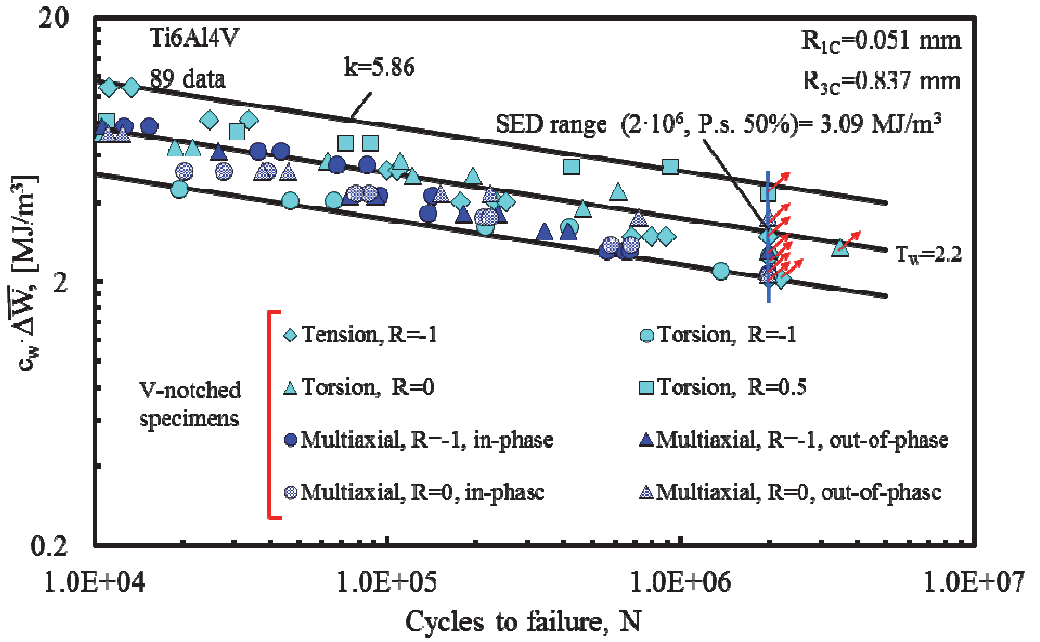

Figure 18: Synthesis by means of local SED of V-notched specimens' data.

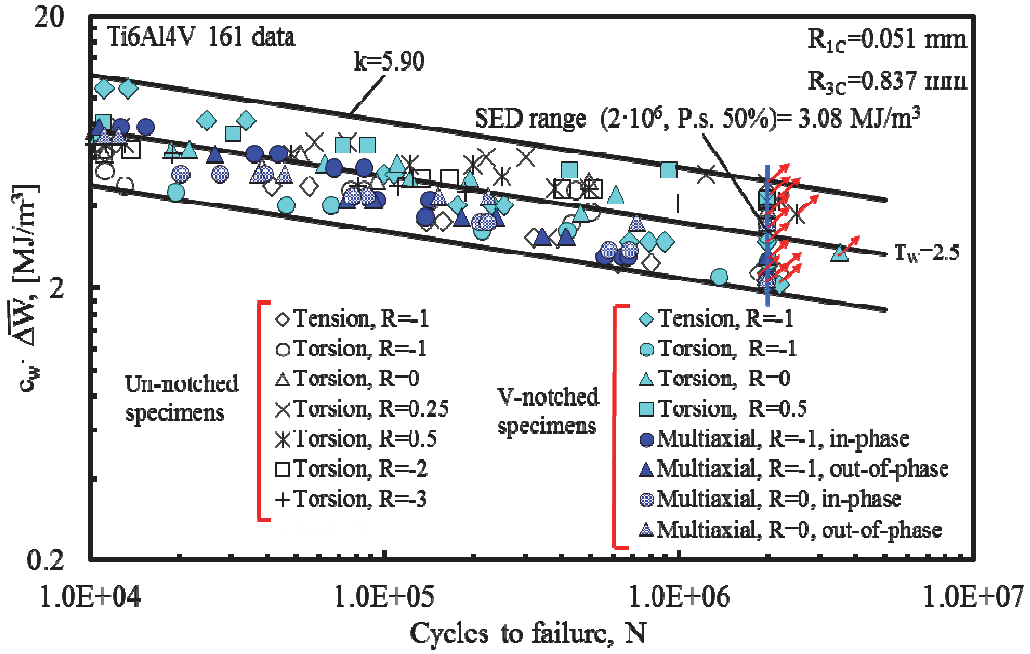

Figure 19: Synthesis by means of local SED of un-notched and V-notched specimens' data.

Dealing with Cu-Be alloy recently investigated, the fatigue data are plotted in terms of averaged strain energy density range over a control volume in Fig. 21 [122], considering a critical radius equal to 0.6 mm. Thanks to the SED approach it has been possible to summarize in a single scatterband all the fatigue data, independent of the specimen geometry, estimating also the characteristic radius for the considered material at high temperature.

More recent data from 40CrMoV13.9 data from unnotched and notched specimens have been summarized by using the SED approach. On the basis of the experimental evidences of [123], the synthesis in terms of SED has been carried out up to 500°C considering the same critical radius used in Ref. [124] dealing with multiaxial fatigue tests performed on the same material (R_0=0.05 mm). In fact no reduction in the fatigue strength has been detected until 500°C both for unnotched and notched specimens.

(a) (b)

Figure 20: High temperature tests on plain (a) and notched specimens (b).

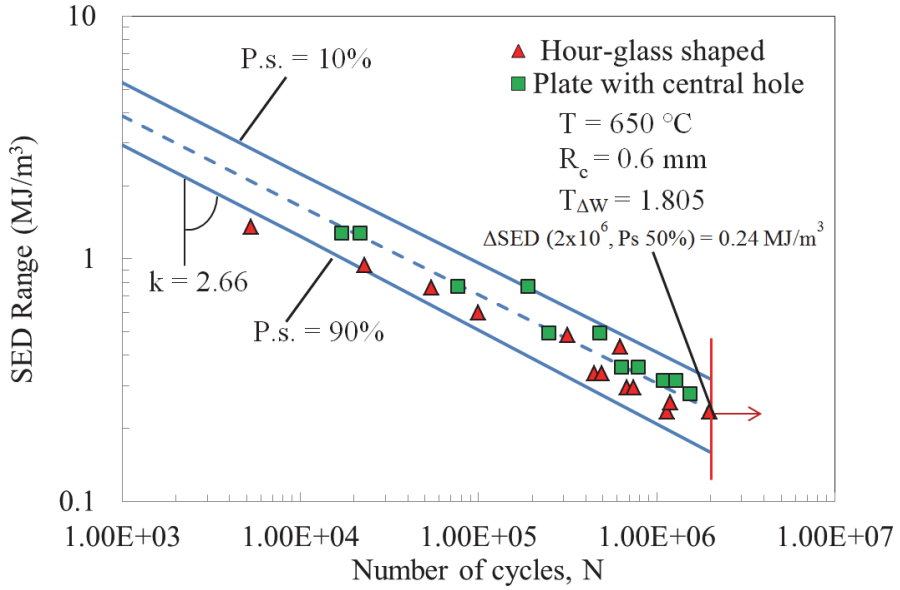

Figure 21: Synthesis by means of local SED of fatigue data from Cu-Be specimens [14].

In the medium and high cycle fatigue regime the critical SED range for un-notched specimens can be simply evaluated by using the following expression:

$$\Delta\bar{W} = \frac{c_w}{2E}\Delta\sigma_n^2 \tag{13}$$

In Eq. (13) $\Delta\sigma_n$ is the nominal stress range referred to the net sectional area. As said above, the weighting parameter c_W has to be applied to take into account different values of the nominal load ratio. Being the actual tests referred to R=0, c_w is equal to 1.0. Being Eq. (13) applied here to different temperatures the Young's modulus has to be updated as a function of the temperature. E is equal to 206 GPa at room temperature and 135 GPa at 650°C. For a temperature of 360°C it results to be 165GPa and at 500°C it is equal to 150 GPa. For notched specimens Eq. (3) can be directly applied. For the specific case of 2α=90° and R_r/ρ=0.05/1 function F is equal to 0.7049 and H is equal to 0.5627, respectively [15, 16]. The stress concentration factor referred to the net area is equal to 3.84.

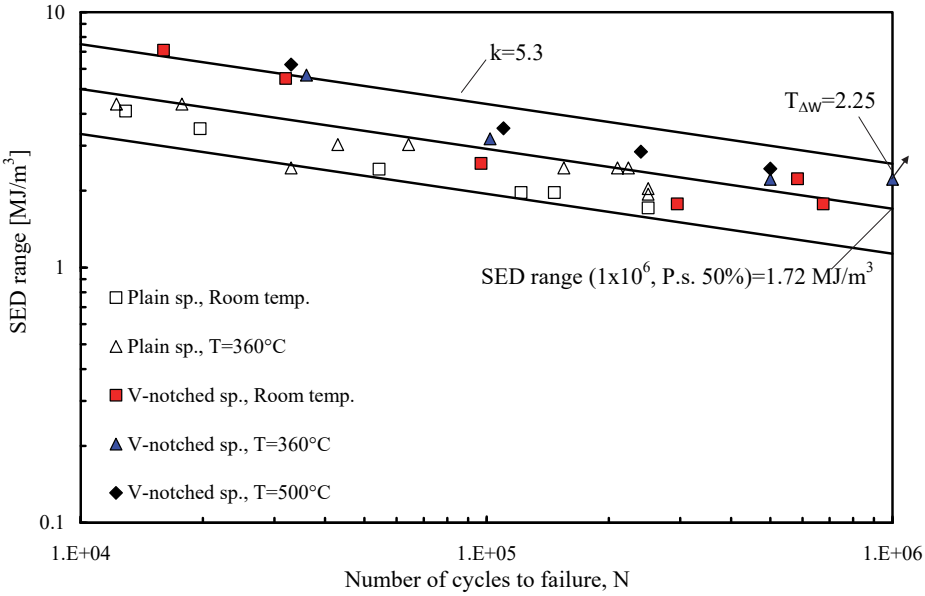

Figure 22: Synthesis by means of local SED of fatigue data in a temperature range between room temperature up to 500°C.

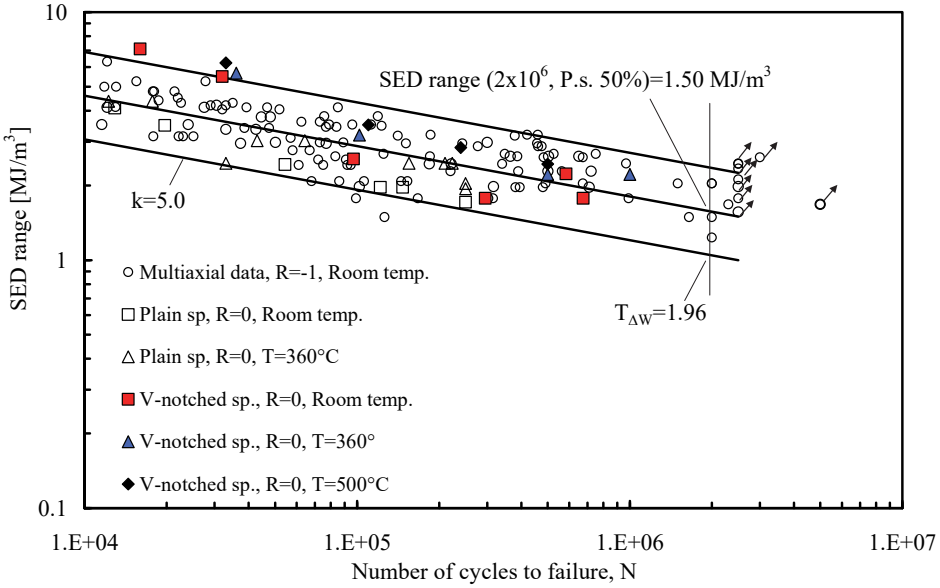

Figure 23: Synthesis by means of local SED of new fatigue data up to 500°C and multiaxial fatigue data.

By using Eq. (3) and Eq. (13) the new data from tests carried out at room temperature up to 500°C can be summarized in a single narrow scatterband characterized by an inverse slope k equal to 4.6 and a scatter index $T_{\Delta W}$, related to the two curves with probabilities of survival P_S= 10% and 90%, equal to 2.1 (see Fig. 22). By converting the data from multiaxial tests on the same material carried out at R=-1, in terms of SED range and by considering c_w=0.5 a single scatterband has obtained, as shown in Fig. 23.

Dealing with data carried out at 650°C, the fatigue strength of un-notched and notched specimens has been found strongly lower than the corresponding data from tests carried out at T<500°C. For this specific temperature (T=650°), which is important in practical industrial applications in particular for hot rolling of aluminum alloys, an empirical formula has been proposed for notched specimens by modifying Eq. (3). This allows us to take into account the notch sensitivity of this material at temperatures higher than 500°C [123]:

$$\Delta\bar{W} = c_w Q(T) L(f/f_0) F(2\alpha) \times H(2\alpha, \frac{R_c}{\rho}) \times \frac{K_{t,n}^2 \Delta\sigma_n^2}{E} \tag{14}$$

Q (T) is the notch sensitivity function at a specific temperature T. This function has to be set (as a function of the temperature T) by equating at high cycle fatigue (10^6 cycles) the SED value from plain specimens and those from notched specimens. f is the test frequency of notched specimens at high temperature and f_0 the test frequency of unnotched specimens at the same temperature. L is a function related to the sensitivity of the material to the load frequency and depends on the ratio f/f_0. Function L is required to be equal to 1.0 if $f=f_0$, which is a condition respected in the actual tests. The critical radius R_0 is kept constant and equal to that obtained at room temperature (R_c=0.05 mm). Dealing with our specific case Q (T=650°C)= 0.18. Eq. (6) can then be re-written by substituting the numerical value of each function [123]:

$$\Delta\bar{W} = 1.0 \times 0.18 \times 1.0 \times 0.7049 \times 0.5627 \frac{K_{t,n}^2 \Delta\sigma_n^2}{E} = 0.07139 \frac{K_{t,n}^2 \Delta\sigma_n^2}{E} \tag{15}$$

For the considered geometry $K_{t,n}$=3.84.

By considering Eq. (15) applied to notched specimens and Eq. (13) applied to plain specimens, the SED master curve for 40CrMoV13.9 at 650°C has been obtained. The fatigue data from tests at 650°C are plotted in terms of averaged strain energy density range over a control volume in Fig. 24, considering the aforementioned critical radius derived from room temperature tests. It is possible to observe that the scatter band is narrow, being the scatter index T_w = 2.6, which is equal to 1.61 when reconverted to an equivalent local stress range. The inverse slope of the scatterband is equal to 1.51. Thanks to the SED approach it is possible to summarize in a single scatterband all the fatigue data at the same temperature, independent of the specimen geometry. Future developments will be devoted to set the proposed empirical equation to other geometries and

temperatures. Moreover, it has been studied for higher temperature the interactions between elevated temperature and creep [125, 126].

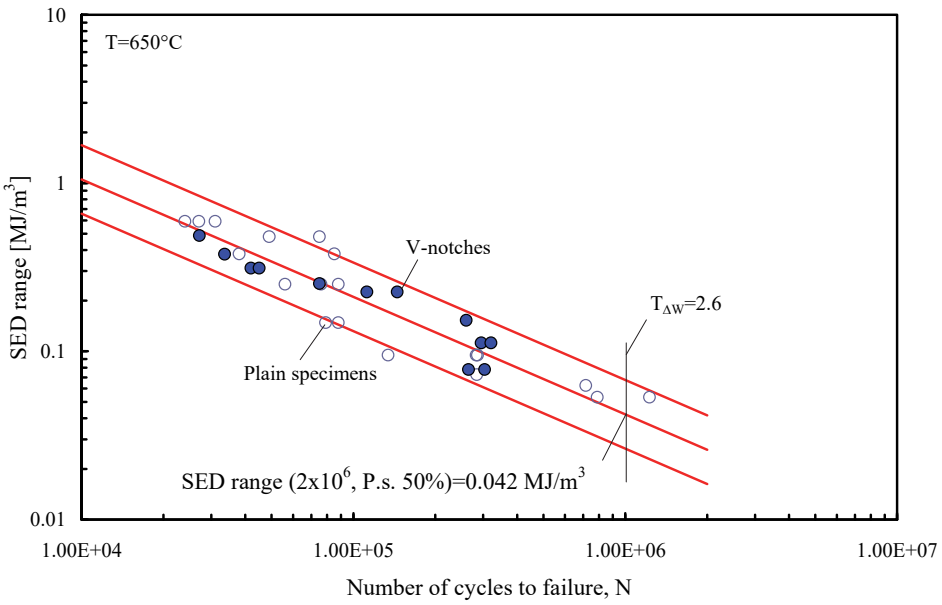

Figure 24: Synthesis by means of local SED of new fatigue data at 650°C. Plain and notched specimens are summarized in the same scatterband.

Fracture at nano-scale level

Fracture mechanics at micro- and nano- scale has become a very attractive topic in the last years [127-136]. However, the results on this topic are still few, mostly because of the lack of effective analytical tools and of the difficult to conduct experimental tests at those scales.

A recent work has reanalyzed experimental tests conducted on nanometer specimens made of single-crystal silicon. The cracking behavior was investigated considering small single-crystal silicon specimens with different precrack lengths, generating singular stress field in the range of 23–58 nm lengths. K_{IC}, was found to be in good agreement with that of the macroscale (bulk) counterpart, clearly indicating that the fracture toughness is independent of the size [136].

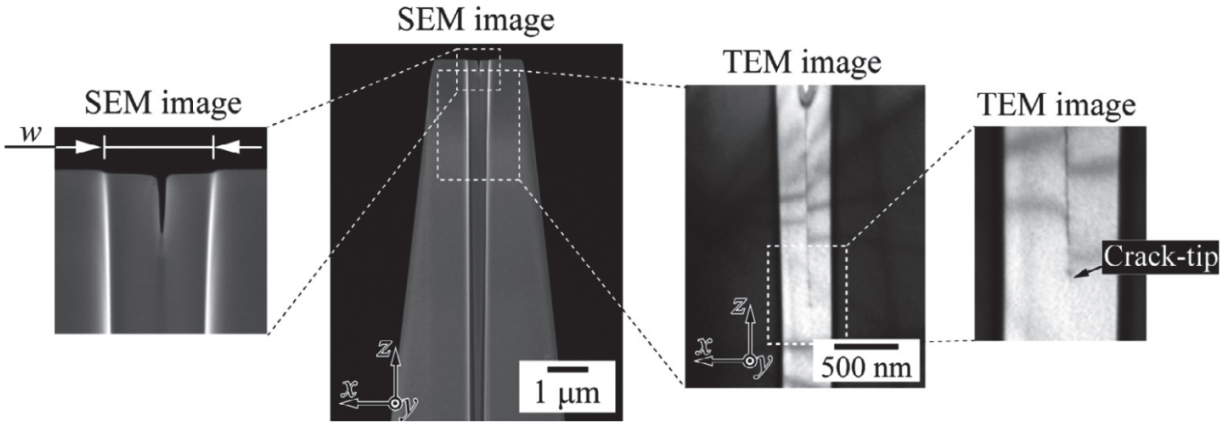

Figure 25: Precrack tip recently studied in [136-137].

In recent studies, the authors reported preliminary analysis on the application of the Strain Energy Density (SED) approach at nano-scale, based on those experimental results [137] (geometry is reported in Fig. 25. Starting from the evaluated mechanical properties, a first evaluation of the control volume due to a nano-size singular stress field has been carried out. Some preliminary considerations on the SED approach at nano-scale have been reported, with emphasis on

the advantages and drawbacks of the method when homogenous and non-homogenous materials are considered (see Tab. 1). If the extension of the SED approach at micro- nano-scale will be given near future, an easy and fast tool to design against fatigue will be provided for micro-devices such as MEMS, resulting in a significant technological impact and providing an easy and fast tool to conduct static and fatigue assessment at micro- and nano-scale.

	K_{IC} (MPa×m$^{0.5}$)	R_c Plane Strain (μm)	R_c Plane Stress (μm)
Spec. 1	0.83	0.48	0.56
Spec. 2	1.09	0.82	0.97
Spec. 3	1.08	0.81	0.95
Spec. 4	1.35	1.26	1.49
Average	1.09	0.84	0.99

Table 1: Fracture toughness K_{IC}, and evaluated control radii R_c for plane strain and plain stress condition.

The applications to micro-systems can take advantage of the application of the SED approach. In fact the miniaturization of electronic and mechanical devices due to the increase of integration and energy saving has pushed the size of components approaching smaller dimension: micro-electro-mechanical systems (MEMS) including small sensors for propulsion and power are good examples.
The small dimensions of micro/nanomaterials impose a tremendous challenge for the experimental study of their mechanical properties that prevent a fast development of theoretical and numerical tools for the design of those components.
The following main conclusions have been drawn in [137]:

- Under very small scales (such as nano- micro- scale), the homogeneity of the bodies return to be present in some cases, giving promising good perspectives on the applicability of SED at those scales;
- Single crystal silicon, thanks to its brittle behavior until failure at room temperature and to its large widespread use, is particularly appropriate to conduct preliminary analyses;
- Employing the mechanical properties experimentally evaluated, a control volume equal to 0.84 μm and 0.99 μm has been theoretically evaluated under plane stress and plane strain condition, respectively, for a single crystal Si;
- A value of critical strain energy density W_c=15.38 MJ/m^3 for static assessment has been provided for a single crystal Si;
- The lack in the literature regarding the experimental study of the mechanical properties of such components prevent a fast development of theoretical and numerical tools;
- The control radius and critical energy provided are the first step to consider further extension of the method to micro and nano scales although difficulties arise when dealing with experimental characterization;
- The obtained critical radius should be also applied to other micro materials, verified that the hypothesis of homogeneity is satisfied;
- In case of materials inhomogeneity, adoption of multiscaling scheme can be considered

Further analyses should be devoted in the investigation of the static and fatigue assessment of notched component made of Si at micro scale, in order to verify that, also at small scales, the Strain Energy Density averaged over a control volume can summarize in a single narrow scatter band all the data, regardless of the notch geometry.

Fatigue behavior of additive manufacturing materials

In the ambit of continuous digitalization of manufacturing processes, modern short product life cycles and the ever-growing need for high performance, low weight products with minimal production needs, we face stringent requirements on both time and sophistication of modern structural design and property prediction. For digital production and advanced components of the future, conventional design methods, structural evaluation routines and production techniques fail to fulfil necessary requirements for structural complexity leading to increased performance. The autonomous production in the ambit of the 4th industrial revolution paired with the need for parts that challenge today's production constraints necessitate the use of enabling technologies such as additive manufacturing (AM). These technologies allow the direct conversion of digital designs into physical products within one production step and completely autonomous avoiding

setup time and the use of tools (Fig. 26). This digital workflow prompts a product development process and structural property prediction without physical testing, only utilizing advanced simulation based methods for both, structural optimization and failure prevention.

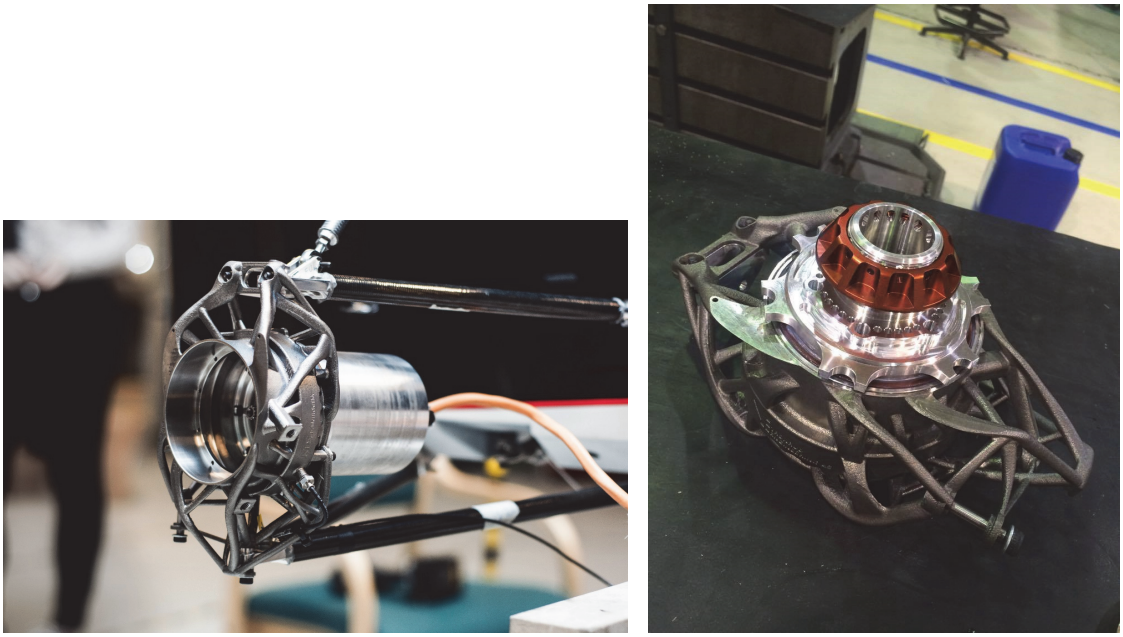

Figure 26: Complex component obtained by AM processes.

With AM, however, a significant problem arises in these methodologies. In conventional manufacturing technologies, one utilizes a given material with defined and well-known material properties and removes material to obtain the desired geometry. In contrast, the material properties in AM evolve during the fabrication process. Geometry and material properties are closely related, every change in the geometry will change the way the AM machine performs its building routine affecting the toolpath and ultimately the properties of the resulting solid. Parts are no longer isotropic, in some cases not fully dense, surfaces are rough and there is a high change of inclusions, impurities and inhomogeneities, all related to the underlying manufacturing strategy, which, in turn, is dependent on the input geometry.
We face a dilemma; on the one hand, we possess a technology that is undoubtedly of high potential and can fulfil the needs of modern digital manufacturing, which enables the manufacturing of unprecedented complex designs in an economic fashion. On the other hand, we cannot guarantee that these parts will withstand complex loading scenarios because of the still poor and/or poorly known material properties as well as the failure criteria allowing their prediction in place to date and an accurate design considering the structural integrity is fully guaranteed.
Utilizing modern AM, the aim is to create digital material designs fulfilling stringent requirements of aerospace, automotive and biomedical applications. The latest topology optimization routines can be used and developed further for better usability and better interaction with the AM manufacturing process chain. Specifically, it is possible to work on improving the interfaces between the topology optimization routine and its compatibility to solid modelling. This will enable easy downstream processing. Further, it is necessary to optimize the tessellation routines streamlining the entire development process and allowing smooth transition between the individual steps of the process. Further, it is important to optimize support structures. These are necessary for attaching AM parts to the building platform to ensure dimensional accuracy. These support elements can be considered as part of the optimization routine maximizing speed and minimizing failure already happening in the building process.
To develop experimental and theoretical understanding of the fatigue and fracture behavior of these advanced geometric complex components is then a fundamental step for taking advantage of AM processes in structural components. To date, this assessment and the quality assurance of AM components is not accurate as microstructural features as well as the specific mechanical/cracking behavior of AM materials cannot be modelled effectively due to their building strategy determined microstructural configuration. For complex AM components, no specific design criteria are in place considering stress concentration phenomena arising from geometrical discontinuities/features. Further, no fatigue data generated by testing such geometrical discontinuous AM metals can be found in the technical literature. It remains a very

strategic point to fill this knowledge gap allowing future applicants to take full advantage of the unique features of AM, which will be key to integrate AM in every-day manufacturing. Drawing from extensive expertise in the development of modern fatigue assessment criteria, the trend should be to contribute to the fundamental understanding of the mechanical/cracking behavior of AM metals subjected to fatigue loading as well as the integration of this knowledge in an innovative design methodology. The key feature of this unifying approach is the consideration of microstructural features (such as porosity, grain shape, defect morphology, etc.) of the material near crack initiation locations.

Due to the geometric complexity of AM advanced components and materials, related structures naturally have large surface to volume ratios. Large areas are exposed to and interact with the surrounding, which is even further enhanced through the typically rough surfaces AM parts exhibit. This can be beneficial, as for example in biomedical applications, where cells tend to easily attach to the porous and rough structure of AM fabricated implants finding proper anchor points. However, this exposure can also lead to detrimental effects such as corrosion, environmental induced embrittlement or wear through friction. Independent from the application, the ability to tailor surface characteristics and surface material properties of these advanced geometric complex components, will allow for the ultimate design freedom. Internal defects are very critical for AM parts and compete in creating provisional crack initiation points (see Fig. 27) competing with geometrical discontinuities due to the complexity of the geometrical features need to be designed.

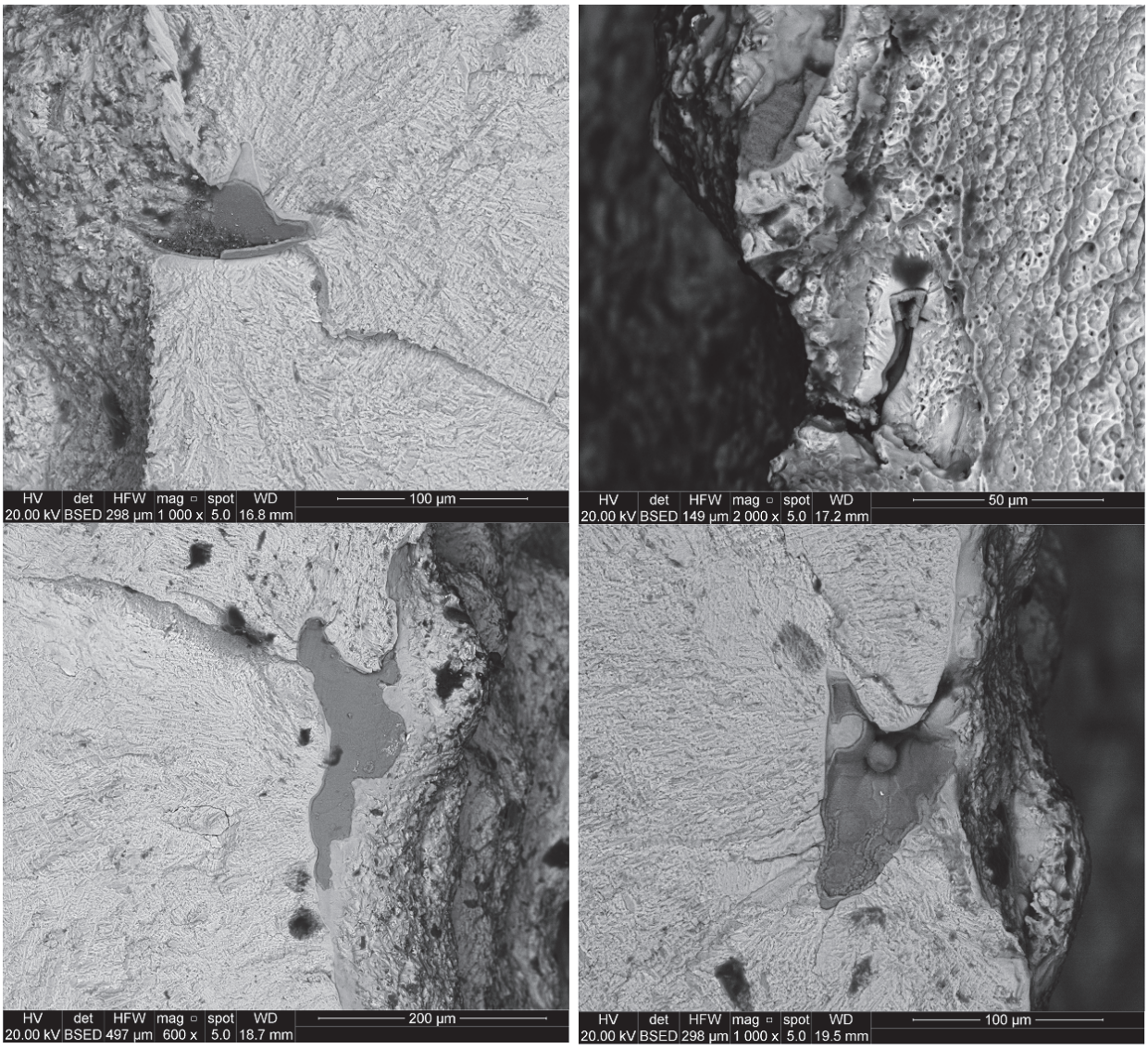

Figure 27: Typical surface intrusions induced by the SLM process.

In SLM-processed samples, fatigue cracks were observed to initiate on severe surface intrusions due to the high roughness induced by the process itself as shown in Fig. 27. Such intrusions are covered by an oxide layer which was formed during the stress-relief heat treatment and non-cleaned up by the grinding treatment. The number of potential crack initiation intrusions is thought to be much higher in smooth samples than in the sharp V-notch specimen where there is the possibility that no such critical surface defects occur in the small region near the notch tip. As discussed in section 4.2 the SED is able to treat in simple and unified way internal defects and notches providing a sound approach for fracture and fatigue assessment of components weakened by defects and notches of any shape. Some preliminary results are reported in Refs. [138-140].

One of the future aim will be to combine AM with thin film deposition [141-143] reaping these technologies' advantages while bypassing their limitations. The final aim should be to fully equip parts with mechanical and electrical properties that are conventionally not achievable, not in costs nor in performance introducing key surface properties ranging from corrosion to scratch resistance, hydrophobicity all the way to enhanced flow characteristics.

In summary, the following three points should be accurately considered: simulation based design, property prediction of additive manufactured parts and thin film deposition. All fields together will enable novel digital materials and designs, their direct conversion into physical parts as well as the guarantee of their compliance through properly defined and tailored failure criterions. This interdisciplinary and integrative research will streamline the digital manufacturing workflow all the way from the idea to the final product and will enable designers and engineers to better transform their ideas into reality.

Hybrid Metal & Extrusion Bonding

Finally, the last potential application of the SED approach that authors want to present in this manuscript is Hybrid Metal & Extrusion Bonding (HYB) [144-147]. The HYB process, developed by Professor Øystein Grong, Engineers Ulf Roar Aakenes and Tor Austigard, is a revolutionary way to achieve bonding without melting base material, thus belonging to cold welding processes. A comprehensive work about the HYB process has been done in Ulf Aakenes' PhD thesis [146], with following images extracted from that work. To remember is that this first approach is only focused on similar welding, in this case Al alloys.

The idea is to force an extruded plasticized Al (AA6082-T4) wire between two Al plates (AA6082-T6) in a butt join configuration, Fig. 28. The result is an achieved bonding performed by scratching and subsequently restoring the lattice action of the FM. Inside the spindle extruder, at above say 275°C, the FM is submitted to a work hardening process that increases its hardness enough to scrape a thin layer of the BM and overtake the sufficient pressure to promote the joint. A steel scraper was implemented to reshape a V-groove with oxide-free surfaces soon before the aluminum injection, due to back-annealing occurring inside the spindle chamber.

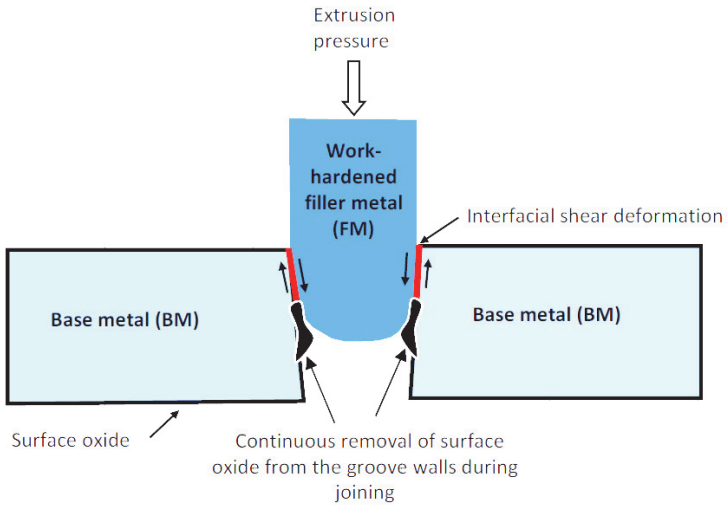

Figure 28: HYB configuration used for similar Al-Al welding.

After years of tests and upgrades, Fig. 29 finally shows the complete workbench used in the experimental activity. The process was performed at room temperature, the heat generated belongs only to the strain work inside the spindle extruder. Two plates of 4mm 6082-T6 Al alloy were used in the experiments.

Figure 29: Experimental setup of Al-Al HYB configuration: HYB spindle extruder (2), steel fixture (3), and aluminum plates to be welded (6).

Some of the final results are shown in Fig. 30, and confirm a good joint appearance.
Still some work needs to be carried out, since some crack-like defects are evident, which demands that both equipment and control software be upgraded.
The potential of this technology is very high and it should be considered to expand the capabilities of the HYB machine. The idea could be raising the possibilities by simply changing the spindle and its mount. By doing so, the machine would become multipurpose considering additive manufacturing and hybrid welding applications. The main advantages given by this new way of joining should be increasing quality and efficiency of overall welding properties, where less amount of energy is wasted than that in other processes, by decreasing temperatures as well. Critical is understanding how materials react in this process.

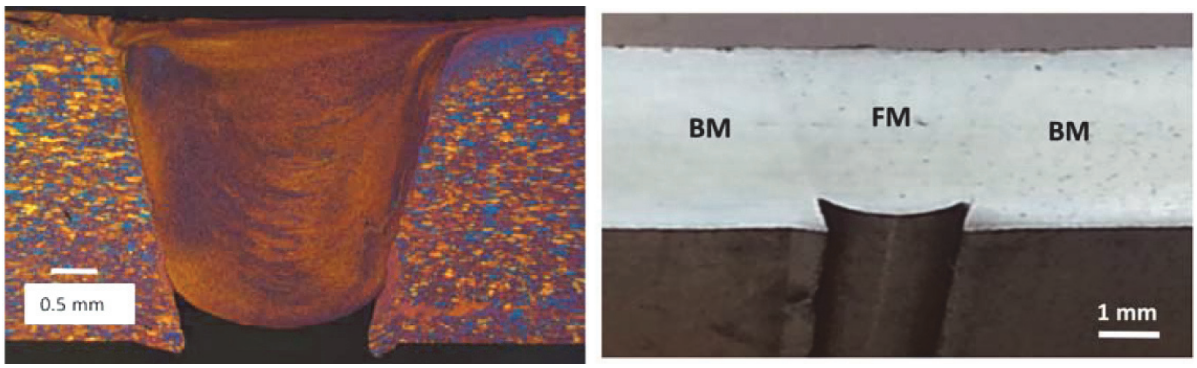

Figure 30: Optical macrograph of the joint cross section.

The HYB machine has been modified by mounting a different spindle extruder. During the welding procedure, the aluminum and steel butt plates are fixed leaving a little gap between them. The butt surface of the steel plate has been previously beveled and fixed leaving 2 mm of space from the center of the welding, while the aluminum plate presents a vertical surface, Fig. 31. This spindle extruder has a specific shape, capable of squeezing plasticized aluminum in the gap between the plates while moving the material close to it. In this way, the tool operates also a strain work on the aluminum side. This new version of the spindle extruder has been called PinPoint spindle.

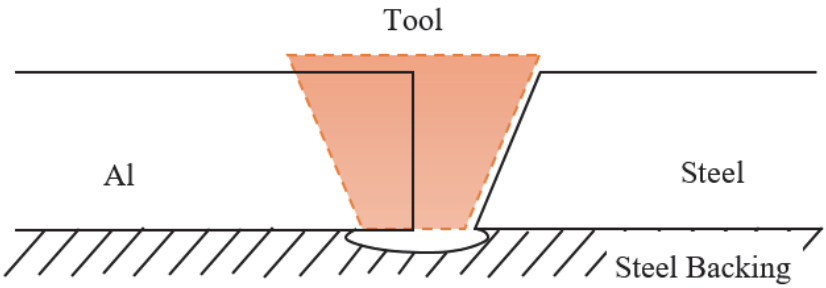

Figure 31: Sketch, not in scale, of how the HYB's tool works the material to obtain the welding. The aluminum side is deformed by the tool while the steel side remains untouched.

The welding is therefore achieved by the synergic action of two processes. The first one is the filling action of the extruded material, which will fully fill up the void between the plates, scrape off the oxide layer and deform the Al BM by shear stresses. The second is the rotating process of the spindle tool that contributes to the mixing of the FM with aluminum taken from the butt plate by the tool, which will enhance metal surface exposure. This takes the oxides issue out and promotes virgin surface contacts, as new metal is continuously exposed. Fig. 32 reveals how the upper shape of the welding presents characteristic periodic curves due to the spindle rotation. The transversal view shows the flash on the top and the clean root shape on the bottom of the joint. The beveled steel butt plate shows a clear straight welded line, not being touched by the spindle itself during the entire process.

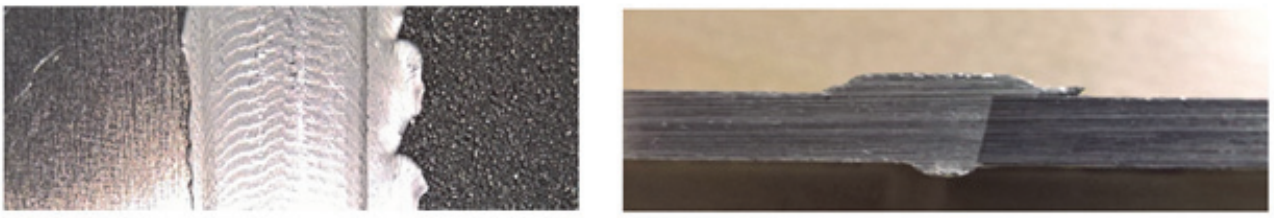

Figure 32: Upper and transversal appearance of HYB dissimilar welded plates. Aluminum on left side, steel on the right side.

Figs. 33 and 34 show the details of Al-steel joints recently obtained in [147]. This new method of joining parts is very promising and the structural integrity, in particular fracture and fatigue behavior have been initially studied in [147] showing some good potential also in this sense. The design of these joints remain a challenging point that can be faced with the application of the SED approach.

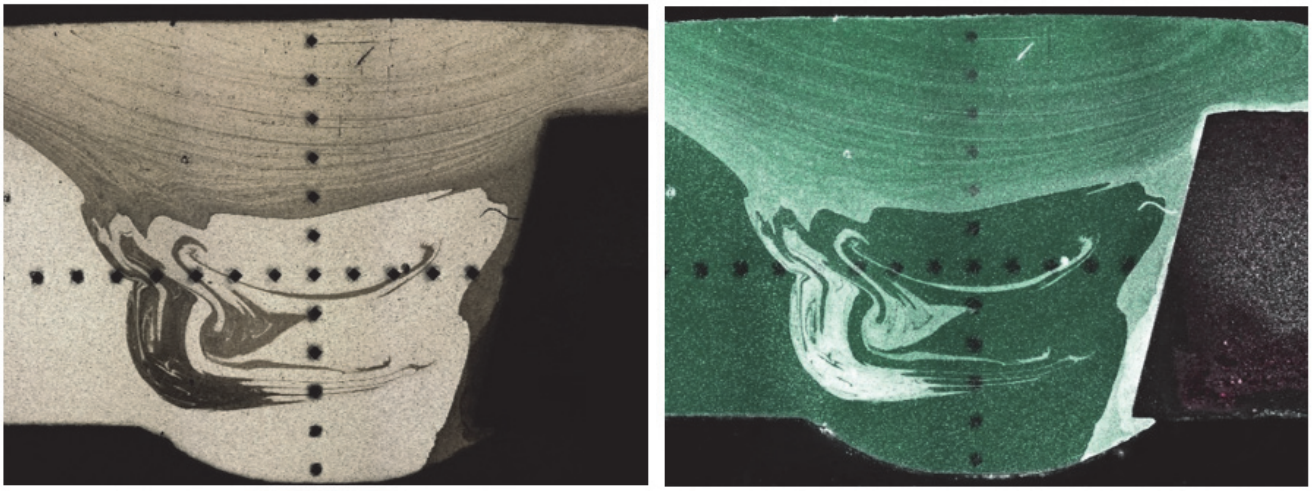

(a) (b)

Figure 33: HYB weldments. The first with normal light (a), the second with polarized light (b).

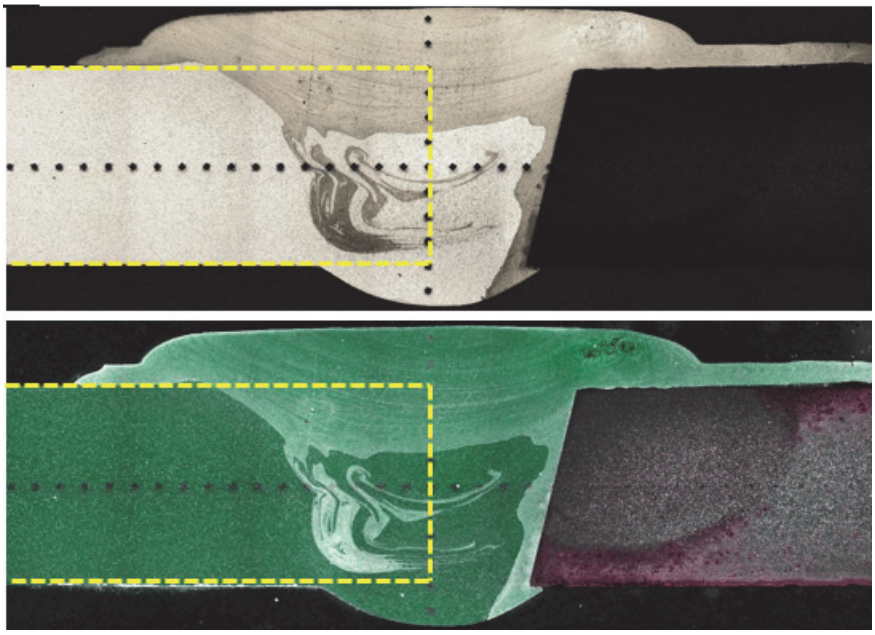

Figure 34: Other images of the weld, both with normal and polarized light. The dashed yellow line represents the initial shape of the aluminum plate, before the welding process.

Conclusions

For many years the Strain Energy Density (SED) has been used to formulate failure criteria for materials exhibiting both ductile and brittle behavior. SED is the most fundamental quantity in Mechanics being all physical quantities expressible in terms of it. From pico- to macroscopic scale the energy absorption and dissipation can explain the most complex phenomena tied to fracture initiation and propagation.

Keeping in mind that the design rules valid for large bodies (i.e high volume to surface ratio) cannot be directly translated and applied to small bodies where local inhomogeneities play a fundamental role for the material damage initiation and propagation and being also aware of the recent contributions and efforts to develop a multiscaling and segmentation scheme able to capture the complex phenomena that happen at every level from pico to macro, the main purpose of the paper is to present a review of the approach based on the mean value of the local strain energy density.

Dealing with static loading the approach is applied here to different materials and geometries both, under mode I and mixed mode (I+II) loading. About one thousand experimental data, taken from the recent literature, are involved in the synthesis. They were from U- and V-notched specimens made of very different materials. A scatter band is proposed by using as a synthesis parameter the value of the local energy averaged over control volume (of radius R_0), normalized by the critical energy of the material. Such a normalized energy is plotted as a function of the notch radius to critical radius ratio, R/R_0.

The strain energy density (SED) in a circular sector of radius R_0 located at the crack initiation sites has successfully been used to summarize also about nine hundred data from fatigue failures of welded joints.

Under the hypothesis that all material inhomogeneities can be averaged, that ceases to be valid at pico- and micro-levels but at the same time is the basis of the volume-based theories applied to structural components, the Strain Energy Density Approach is shown to be a powerful tool both for static and fatigue strength assessment of notched and welded structures.

References

[1] Tang, X.S., Sih, G.C., Weak and strong singularities reflecting multiscale damage: Micro-boundary conditions for free–free, fixed–fixed and free–fixed constraints, Theor. Appl. Fract. Mech., 43 (2005) 5-62.

[2] Sih, G.C., Tang, X.S., Scaling of volume energy density function reflecting damage by singularities at macro-, meso- and microscopic level, Theor. Appl. Fract. Mech., 43 (2005) 211-231.
[3] Sih, G.C., Multiscaling in molecular and continuum mechanics: interaction of time and size from macro to nano. Dordrecht: Springer; 2007.
[4] Sih, G.C., Crack tip mechanics based on progressive damage of arrow: Hierarchy of singularities and multiscale segments, Theor. Appl. Fract. Mech., 51 (2009) 11-32
[5] Sih, G.C., Ideomechanics of transitory and dissipative systems associated with length, velocity, mass and energy, Theor. Appl. Fract. Mech., 51 (2009) 149-160.
[6] Sih, G.C., Energy absorption and dissipation associated with mass activation and deactivation for open systems, Theor. Appl. Fract. Mech., 52(2) (2009) 63-71.
[7] Lazzarin, P., Zambardi, R., A finite-volume-energy based approach to predict the static and fatigue behaviour of components with sharp V-shaped notches, Int. J. Fract., 112 (2001) 275-298.
[8] Lazzarin, P., Lassen, T., Livieri, P., A Notch Stress Intensity approach applied to fatigue life predictions of welded joints with different local toe geometry, Fatigue Fract. Eng. Mater. Struct., 26 (2003) 49-58.
[9] Lazzarin, P., Sonsino, C.M., Zambardi, R., A notch stress intensity approach to assess the multiaxial fatigue strength of welded tube-to flange joints subjected to combined loadings, Fatigue Fract. Eng. Mater. Struct., 27 (2004) 127-140.
[10] Livieri, P., Lazzarin, P., Fatigue strength of steel and aluminium welded joints based on generalised stress intensity factors and local strain energy values, Int. J. Fract., 133 (2005) 247-278.
[11] Lazzarin, P., Berto, F., Some expressions for the strain energy in a finite volume surrounding the root of blunt V-notches, Int. J. Fract., 135 (2005) 161-185.
[12] Lazzarin, P., Berto, F. From Neuber's elementary volume to Kitagawa and Atzori's diagrams: an interpretation based on local energy, Int. J. Fract., 135 (2005) L33-L38.
[13] Lazzarin, P., Livieri, P., Berto, F., Zappalorto, M., Local strain energy density and fatigue strength of welded joints under uniaxial and multiaxial loading, Eng. Fract. Mech., 75 (2008) 1875-1889.
[14] Lazzarin, P., Berto, F., Control volumes and strain energy density under small and large scale yielding due to tensile and torsion loading, Fatigue Fract. Eng. Mater. Struct., 31 (2008) 95-107.
[15] Berto, F., Lazzarin, P., A review of the volume-based Strain Energy Density approach applied to V-notches and welded Structures, Theor. Appl. Fract. Mech., 52 (2009) 183-194.
[16] Berto, F., Lazzarin, P., Recent developments in brittle and quasi-brittle failure assessment of engineering materials by means of local approaches, Mater. Sci. Eng. R, 75 (2014) 1-49.
[17] Neuber, H., Kerbspannungslehre. Springer-Verlag, Berlin, (1958) 2nd edn.
[18] Neuber, H., Űber die Berücksichtigung der Spannungskonzentration bei Festigkeitsberechnungen, Konstruktion 20 (1968) 245-251.
[19] Neuber, H., Kerbspannungslehre. Springer-Verlag, Berlin, (1985) 3rd edn.
[20] Radaj, D., Näherungsweise Berechnung der Formzahl von Schweißnähten. Schw Schn, 21 (1969) 97-105 and 21 (1969) 151-158.
[21] Radaj, D., Design and Analysis of Fatigue Resistant Welded Structures, Cambridge: Abington Publishing; (1990).
[22] Radaj, D., Ermüdungsfestigkeit, 2nd ed. Berlin: Springer Verlag; (2003).
[23] Radaj, D., Sonsino, C.M., Fricke, W., Fatigue Assessment of Welded Joints by Local Approaches, 2nd ed. Cambridge: Woodhead Publishing; Boca Raton, FL: CRC Press; (2006).
[24] Berto, F., Fictitious notch rounding concept applied to V-notches with end holes under mode 3 loading, Int. J. Fatigue, 38 (2012) 188–193.
[25] Berto, F., Lazzarin, P., Radaj, D., Fictitious notch rounding concept applied to V-notches with root holes subjected to in-plane shear loading, Eng. Fract. Mech., 79 (2012) 281-294.
[26] Radaj, D., Lazzarin, P., Berto, F., Generalised Neuber concept of fictitious notch rounding, Int. J. Fatigue, 51 (2013) 105-115.
[27] McClintock, F.A., Ductile fracture instability in shear, J. Appl. Mech., 25 (1958) 582-588.
[28] Ritchie, R.O., Knott, J., Rice, J.R., On the relation between critical tensile stress in fracture toughness in mild steel, J. Mech. Phys. Solids, 21 (1973) 395-410.
[29] Knésl, Z., A criterion of V-notch stability, Int. J. Fract., 48 (1991) R79-R83.
[30] Seweryn, A., Brittle fracture criterion for structures with sharp notches, Eng. Fract. Mech., 47 (1994) 673-681.
[31] Novozhilov, V.V., On necessary and sufficient criterion of brittle fracture, Prikladnaja Matematika i Mechanika 33 (1969) 212-222.

[32] Seweryn, A., Mróz, Z., A non-local stress failure condition for structural elements under multiaxial loading, Eng. Fract. Mech., 51 (1995) 955-973.
[33] Seweryn, A., Poskrobko, S., Mróz, Z., Brittle fracture in plane elements with sharp notches under mixed-mode loading, J. Eng. Mech., 123 (1997) 535-543.
[34] Sheppard, S.D., Field effects in fatigue crack initiation: long life fatigue strength, Trans. ASME. J. Mech. Des., 113 (1991) 188-194.
[35] Beltrami, E., Sulle condizioni di resistenza dei corpi elastici, Rend. R. Ist. Lombardo di Scienze, Lettere e Arti, 18 (1885) 704 (in Italian).
[36] Sih, G.C., A special theory of crack propagation: methods of analysis and solutions of crack problems, Mechanics of Fracture, edited by GC Sih, Noordhoff, International Publishing, Leyden, (1973) 21-45.
[37] Sih, G.C., Strain-energy-density factor applied to mixed mode crack problems, Int. J. Fract., 10 (1974) 305-321.
[38] Sih, G.C., Surface layer energy and strain energy density for a blunted crack or notch, Prospect of Fracture Mechanics, edited by GC Sih, HC van Elst and D Broek, Noordhoff International Publishing, Leyden, (1974) 85-102.
[39] Sih, G.C., Mechanics of Fracture Initiation and Propagation: Surface and volume energy density applied as failure criterion, Kluwer Academic Publisher, Dordrecht (1991).
[40] Sih, G.C., Ho, J.W., Sharp notch fracture strength characterized by critical energy density, Theor. Appl. Fract. Mech., 16 (1991) 179-214.
[41] Sih, G.C., Czoboly, E., Gillemot L.F., Absorbed Specific Energy and Strain Energy Density Criterion, Proceedings of an International Symposium on Absorbed Specific Energy and Strain Energy Density Criterion, Budapest, September 1980. In memory of the late Professor László Gillemot, Martinus Nijhoff Publishers, (1982), The Netherlands
[42] Gillemot, L.F., Brittle fracture of welded materials. In: Commonwealth Welding Conference C.7, (1965) 353-358.
[43] Gillemot, L.F., Criterion of crack initiation and spreading. Engineering Fracture Mechanics, 8 (1976) 239-253.
[44] Gillemot, L.F., Czoboly, E., Havas, I., Fracture mechanics applications of absorbed specific fracture energy: notch and unnotched specimens, Theor. Appl. Fract. Mech., 4 (1985) 39-45.
[45] Glinka, G., Molski, K., A method of elastic-plastic stress and strain calculation at a notch root, Mater. Sci. Eng., 50 (1981) 93-100.
[46] Glinka, G., Energy density approach to calculation of inelastic strain-stress near notches and cracks, Eng. Fract. Mech., 22 (1985) 485-508.
[47] Ellyin, F., Fatigue Damage, Crack Growth and Life Prediction, London, Chapman & Hall (1997).
[48] Ellyin, F., Kujawski, D., Generalization of notch analysis and its extension to cyclic loading, Eng. Fract. Mech., 32 (1989) 819-826.
[49] Yosibash, Z., Bussiba, A., Gilad, I., Failure criteria for brittle elastic materials, Int. J. Fract., 125 (2004) 307-333.
[50] Kipp, M.E., Sih, G.C., The strain energy density failure criterion applied to notched elastic solids, Int. J. Solids Struct., 11 (1975) 153–173.
[51] Carpinteri, A., Stress singularity and generalised fracture toughness at the vertex of re-entrant corners, Eng. Fract. Mech., 26 (1987) 143-155.
[52] Nui, L.S., Chehimi, C., Pluvinage, G., Stress field near a large blunted tip V-Notch and application of the concept of the critical notch stress intensity factor (NSIF) to the fracture toughness of very brittle materials, Eng. Fract. Mech., 49 (1994) 325-335.
[53] Gómez, F.J., Elices, M., Valiente, A., Cracking in PMMA containing U-shaped notches, Fatigue Fract. Eng. Mater. Struct., 23 (2000) 795-803.
[54] Atzori, B., Lazzarin, P., Notch sensitivity and defect sensitivity: two sides of the same medal, Int. J. Fract., 107 (2001) L3-L8.
[55] Strandberg, M., Fracture at V-notches with contained plasticity, Eng. Fract. Mech., 69 (2002) 403-415.
[56] Atzori, B., Lazzarin, P., Meneghetti, G., Fracture mechanics and notch sensitivity, Fatigue Fract. Eng. Mater. Struct., 26 (2003) 257-267.
[57] Gogotsi, G.A., Fracture toughness of ceramics and ceramic composites, Ceram. Int., 7 (2003) 777-884.
[58] Leguillon, D., Yosibash, Z., Crack onset at a V-notch. Influence of the notch tip radius, Int. J. Fract., 122 (2003) 1-21.
[59] Dini, D., Hills, D., Asymptotic characterisation of nearly-sharp notch root stress fields, Int. J. Fract., 130 (2004) 651-666.
[60] Yosibash., Z., Priel, E., Leguillon, D., A failure criterion for brittle elastic materials under mixed-mode loading, Int. J. Fract., 141 (2006) 291-312.
[61] Leguillon, D., Quesada, D., Putot, C., Martin, E., Prediction of crack initiation at blunt notches and cavities – size effects, Eng. Fract. Mech., 74 (2007) 2420-2436.

[62] Gómez, F.J., Elices, M., Fracture of components with V-shaped notches, Eng. Fract. Mech., 70 (2003) 1913-1927.
[63] Gómez, F.J., Elices, M., A fracture criterion for sharp V-notched samples, Int. J. Fract., 123 (2003) 163-175.
[64] Gómez, F.J., Elices, M., A fracture criterion for blunted V-notched samples, Int. J. Fract., 127 (2004) 239-264.
[65] Gómez, F.J., Elices, M., Planas, J., The cohesive crack concept: application to PMMA at –60°C, Eng. Fract. Mech., 72 (2005) 1268-1285.
[66] Theocaris, P.S., A higher order approximation for the T-criterion of fracture in biaxial fields, Eng. Fract. Mech., 19 (1984) 975-991.
[67] Ayatollahi, M.R., Aliha, M.R.M., Analysis of a new specimen for mixed mode fracture tests on brittle materials, Eng. Fract. Mech., 76 (2009) 1563-1573.
[68] Ayatollahi, M.R., Torabi, A.R., Determination of mode II fracture toughness for U-shaped notches using Brazilian disc specimen, Int. J. Solids Struct., 47 (2010) 454-465.
[69] Ayatollahi, M.R., Torabi, A.R., Investigation of mixed mode brittle fracture in rounded-tip V-notched components, Eng. Fract. Mech., 77 (2010) 3087-3104.
[70] Gómez, F.J., Elices, M., Berto, F., Lazzarin, P., Local strain energy to assess the static failure of U-notches in plates under mixed mode loading, Int. J. Fract., 145 (2007) 29-45.
[71] Berto, F., Lazzarin, P., Gomez, F.J., Elices, M., Fracture assessment of U-notches under mixed mode loading: Two procedures based on the 'equivalent local mode I' concept, Int. J. Fract., 148 (2007) 415-433.
[72] Lazzarin, P., Berto, F., Elices, M., Gómez, J., Brittle failures from U- and V-notches in mode I and mixed, I+II, mode. A synthesis based on the strain energy density averaged on finite size volumes, Fatigue Fract. Eng. Mater. Struct., 32 (2009) 671-684.
[73] Gómez, F.J., Elices, M., Berto, F., Lazzarin, P., Fracture of v-notched specimens under mixed mode (I+II) loading in brittle materials, Int. J. Fract., 159(2) (2009) 121-135.
[74] Torabi, A.R., Berto, F., Razavi, S.M.J., Ductile failure prediction of thin notched aluminum plates subjected to combined tension-shear loading, Theor. Appl. Fract. Mech., in press. DOI: 10.1016/j.tafmec.2017.05.003.
[75] Aliha, M.R.M., Berto, F., Mousavi, A., Razavi, S.M.J., On the applicability of ASED criterion for predicting mixed mode I+II fracture toughness results of a rock material, Theor. Appl. Fract. Mech., in press. DOI: 10.1016/j.tafmec.2017.07.022.
[76] Razavi, S.M.J., Aliha, M.R.M., Berto, F., Application of an average strain energy density criterion to obtain the mixed mode fracture load of granite rock tested with the cracked asymmetric four-point bend specimens, Theor. Appl. Fract. Mech., in press. DOI: 10.1016/j.tafmec.2017.07.004.
[77] Williams, M.L., Stress singularities resulting from various boundary conditions in angular corners on plates in tension, J. Appl. Mech., 19 (1952) 526-528.
[78] Lazzarin, P., Berto, F., Control volumes and strain energy density under small and large scale yielding due to tensile and torsion loading, Fatigue Fract. Eng. Mater. Struct., 31 (2008) 95-107.
[79] Lazzarin, P., Berto, F., Gómez, F.J., Zappalorto, M., Some advantages derived from the use of the strain energy density over a control volume in fatigue strength assessments of welded joints, Int. J. Fatigue, 30 (2008) 1345-1357.
[80] Lazzarin, P., Berto, F., Radaj, D., Stress intensity factors of welded lap joints: a comparison between pointed slit based and keyhole notch based models, with extensions to strain energy density and J-integral, Fatigue Fract. Eng. Mater. Struct., 32 (2009) 713-735.
[81] Lazzarin, P., Berto, F., Zappalorto, M., Mean values of the Strain Energy Density from coarse meshes: theoretical bases of a method suitable for rapid calculations of notch stress intensity factors and fatigue strength of welded joints, Int. J. Fatigue, 32 (2010) 1559-1567.
[82] Berto, F., Lazzarin, P., On higher order terms in the crack tip stress field, Int. J. Fract., 161(2) (2010) 221-226.
[83] Berto, F., Lazzarin, P., Multiparametric full-field representations of the in-plane stress fields ahead of cracked components under mixed mode loading, Int. J. Fatigue, 46 (2013) 16-26.
[84] Berto, F., Lazzarin, P., Marangon, C., Brittle fracture of U-notched graphite plates under mixed mode loading, Mater. Des., 41 (2012) 421-432.
[85] Berto, F., Cendon, D.A., Lazzarin, P., Elices, M., Fracture behaviour of notched round bars made of PMMA subjected to torsion at -60°C, Eng. Fract. Mech., 102 (2013) 271-287.
[86] Hartranft, R.J., Sih, G.C., The use of eigenfunction expansions in the general solution of three-dimensional crack problems, J. Math. Mech., 19 (1969) 123–138.
[87] Hartranft, R.J., Sih, G.C., An approximate three-dimensional theory of plates with application to crack problems, Int. J. Eng. Sci., 8 (1970) 711–729.
[88] Pook, L.P., Some implications of corner point singularities, Eng. Fract. Mech., 48 (1994) 367–378.

[89] Pook, L.P., Finite element analysis of corner point displacements and stress intensity factors for narrow notches in square sheets and plates, Fatigue Fract. Eng. Mater. Struct., 23 (2000) 979–992.
[90] Pook, L.P., Crack profiles and corner point singularities, Fatigue Fract. Eng. Mater. Struct., 23 (2000) 141–150.
[91] Pook, L.P., A finite element analysis of cracked square plates and bars under antiplane loading, Fatigue Fract. Eng. Mater. Struct., 26 (2003) 533–541.
[92] Kotousov, A., Lew, T.L., Stress singularities resulting from various boundary conditions in angular corners of plates of arbitrary thickness in extension, Int. J. Solids Struct., 43 (2005) 5100-5109.
[93] Kotousov, A., Fracture in plates of finite thickness, Int. J. Solids Struct., 44 (2007) 8259-8273.
[94] Berto, F., Lazzarin, P., Kotousov, A., On the presence of the out of plane singular mode induced by plane loading with KII = KI = 0, Int. J. Fract., 167 (2011) 119-126.
[95] Berto, F., Lazzarin, P., Kotousov, A., On higher order terms and out-of-plane singular mode, Mech. Mater., 43 (2011) 332–341.
[96] Berto, F., Lazzarin, P., Kotousov, A., Harding, S., Out-of-plane singular stress fields in V-notched plates and welded lap joints induced by in-plane shear load conditions, Fatigue Fract. Eng. Mater. Struct., 34 (2011) 291–304.
[97] Berto, F., Lazzarin, P., Kotousov, A., Pook, P.L., Induced out-of-plane mode at the tip of blunt lateral notches and holes under in-plane shear loading, Fatigue Fract. Eng. Mater. Struct., 35 (2012) 538-555.
[98] Gross, R., Mendelson, A., Plane Elastostatic Analysis of V-Notched Plates, Int. J. Fract. Mech., 8 (1972) 267-227.
[99] Pook, L.P., Berto, F., Campagnolo, A., Lazzarin, P., Coupled fracture mode of a cracked disc under anti-plane loading, Eng. Fract. Mech., 128(C) (2014) 22-36.
[100] Pook, L.P., Campagnolo, A., Berto, F., Lazzarin, P., Coupled fracture mode of a cracked plate under anti-plane loading, Eng. Fract. Mech., 134 (2015) 391-403.
[101] He, Z., Kotousov, A., Berto, F., Effect of vertex singularities on stress intensities near plate free surfaces, Fatigue Fract. Eng. Mater. Struct., 38(7) (2015) 860-869.
[102] Lazzarin, P., Berto, F., From Neuber's Elementary Volume to Kitagawa and Atzori's Diagrams: An Interpretation Based on Local Energy, Int. J. Fract., 135 (2005) L33–L38.
[103] Kitagawa, H., Takahashi, S., Applicability of fracture mechanics to very small cracks in the early stage, Procs. Second International Conference on Mechanical Behaviour of Materials, (1976) 627-631.
[104] Atzori, B., Lazzarin, P., Notch sensitivity and defect sensitivity: two sides of the same medal, Int. J. Fract., 107 (2001) L3-L8.
[105] Atzori, B., Lazzarin, P., Meneghetti, G., Fracture mechanics and notch sensitivity, Fatigue Fract. Eng. Mater. Struct., 26 (2003) 257-267.
[106] El Haddad, M.H., Topper, T.H., Smith, K.N., Prediction of Non-Propagating Cracks, Eng. Fract. Mech., 11 (1979) 573-584
[107] Berto, F., Croccolo, D., Cuppini, R., Fatigue strength of a fork-pin equivalent coupling in terms of the local strain energy density, Mater. Des., 29 (2008) 1780-1792.
[108] Berto, F., Lazzarin, P., Yates, J., Multiaxial fatigue behaviour of quasi-sharp V-notched specimens made of 39NiCrMo3 steel: A non-conventional application of the local energy, Fatigue Fract. Eng. Mater. Struct., 34(11) (2011) 921-943.
[109] Berto, F., Lazzarin, P., Fatigue strength of structural components under multi-axial loading in terms of local energy density averaged on a control volume, Int. J. Fatigue, 33(8) (2011) 1055-1065.
[110] Berto, F. Campagnolo, A., Lazzarin, P. Fatigue strength of severely notched specimens made of Ti–6Al–4V under multiaxial loading Fatigue & Fracture of Engineering Materials & Structures 38 (5), 503-517
[111] Krukemyer, T.H., Fatemi, A., Swindeman, R.W., Fatigue Behaviour of a 22Cr-20Ni-18Co-Fe alloy at elevated temperature, J. Eng. Mater. T Asme, 116 (1994) 54-61.
[112] Kobayashi, H., Todoroki, A., Oomura, T., Sano, T., Takehana, T., Ultra-high-cycle fatigue properties and fracture mechanism of modified 2.25Cr–1Mo steel at elevated temperatures, Int. J. Fatigue, 28 (2006) 1633-1639.
[113] Fan, Z., Chen, X., Chen, L., Jiang, J., Fatigue–creep behavior of 1.25Cr0.5Mo steel at high temperature and its life prediction, Int. J. Fatigue, 29 (2007) 1174-1183.
[114] Ha, T.K., Jeong, H.T., Sung, H.J., High temperature bending fatigue behavior of stainless steels for automotive exhaust, J. Mater. Process Tech., 187 (2007) 555-558.
[115] Uematsu, Y., Akita, M., Nakajima, M., Tokaji, K., Effect of temperature on high cycle fatigue behaviour in 18Cr–2Mo ferritic stainless steel, Int. J. Fatigue, 30 (2008) 642-648.
[116] Fournier, B., Salvi, M., Dalle, F., De Carlan, Y., Caës, C., Sauzay, M., Pineau, A., Lifetime prediction of 9–12%Cr martensitic steels subjected to creep–fatigue at high temperature, Int. J. Fatigue, 32 (2010) 971-978.

[117] Ko, S.J., Kim, Y.J., High temperature fatigue behaviors of a cast ferritic stainless steel, Mat. Sci. Eng. A Struct., 534 (2012) 7-12.
[118] Altenberger, I., Nalla, R.K., Sano, Y., Wagner, L., Ritchie, R.O., On the effect of deep-rolling and laser-peening on the stress-controlled low- and high-cycle fatigue behavior of Ti–6Al–4V at elevated temperatures up to 550 °C, Int. J. Fatigue, 44 (2012) 292-302.
[119] Chen, Q., Kawagoishi, N., Nisitani, H., Evaluation of notched fatigue strength at elevated temperature by linear notch mechanics, Int. J. Fatigue, 21 (1999) 925-931.
[120] Kawagoishi, N., Chen, Q., Nisitani, H., Fatigue strength of Inconel 718 at elevated temperatures, Fatigue Fract. Eng. Mater. Struct., 23 (2000) 209–216.
[121] Shi, D.Q., Hu, X.A., Wang, J.K., Yu, H.C., Yang, X.G., Huang, J., Effect of notch on fatigue behaviour of a directionally solidified superalloy at high temperature, Fatigue Fract. Eng. M, 36 (2013) 1288-1297.
[122] Berto, F., Lazzarin, P., Gallo, P., High-temperature fatigue strength of a copper-cobalt-beryllium alloy, J. Strain Anal. Eng. Des., 49(4) (2013) 244-256.
[123] Berto, F., Gallo, P., Lazzarin, P., High temperature fatigue tests of un-notched and notched specimens made of 40CrMoV13. 9 steel, Mater. Des., 63 (2014) 609-619.
[124] Berto, F., Lazzarin, P., Marangon, C., Fatigue strength of notched specimens made of 40CrMoV13.9 under multiaxial loading, Mater. Des., 54 (2014) 57-66.
[125] Gallo, P., Berto, F., Advanced Materials for Applications at High Temperature: Fatigue Assessment by Means of Local Strain Energy Density, Adv. Eng. Mater., 18 (2015) 2010-2017.
[126] Gallo, P., Berto, F., Glinka, G., Generalized approach to estimation of strains and stresses at blunt V-notches under non-localized creep, Fatigue Fract. Eng. Mater. Struct., 39(3) (2016) 292-306.
[127] Kitamura, T., Sumigawa, T., Hirakata, H. and Shimada, T., Fracture Nanomechanics, Second Edition, Pan Stanford Publishing, Singapore (2015).
[128] Wang, K.F., Wang, B.L., Kitamura, T., A review on the application of modified continuum models in modeling and simulation of nanostructures, Acta Mech. Sin., 32 (2015) 83-100.
[129] Van Truong, D., Van Thanh, V., Hirakata, H., Kitamura, T., Interfacial fatigue fracture criterion of bimaterial in submicron scale, Microelectron. Eng., 140 (2015) 23–28.
[130] Guo, L., Kitamura, T., Yan, Y., Sumigawa, T., Huang, K., Fracture mechanics investigation on crack propagation in the nano-multilayered materials, Int. J. Solids Struct., 64-65 (2015) 208–220.
[131] Fang, H., Shiohara, R., Sumigawa, T., Kitamura, T., Size dependence of fatigue damage in sub-micrometer single crystal gold, Mater. Sci. Eng. A, 618 (2014) 416–423.
[132] Kishimoto, K., Yan, Y., Sumigawa, T., Kitamura, T., Mixed-mode crack initiation at the edge of Cu/Si interface due to nanoscale stress concentration, Eng. Fract. Mech., 96 (2012) 72–81.
[133] Ando, T., Li, X., Nakao, S., Kasai, T., Tanaka, H., Shikida, M., Sato, K., Fracture toughness measurement of thin-film silicon. Fatigue Fract. Eng. Mater. Struct., 28 (2005) 687–694.
[134] Li, X., Kasai, T., Nakao, S., Tanaka, H., Ando, T., Shikida, M., Kazuo, S., Measurement for fracture toughness of single crystal silicon film with tensile test, Sensors Actuators, A Phys., 119 (2005) 229–235.
[135] Shimada, T., Kitamura, T., Fracture Mechanics at Atomic Scales. In: Altenbach, H., Matsuda, T. and Okumura, D. (eds.). Adv. Struct. Mater., 64, Springer International Publishing, Cham, (2015) 379–396.
[136] Sumigawa, T., Ashida, S., Tanaka, S., Sanada, K., Kitamura, T., Fracture toughness of silicon in nanometer-scale singular stress field, Eng. Fract. Mech., 150 (2015) 161–167.
[137] Gallo, P., Sumigawa, T., Kitamura, T., Berto, F., Evaluation of the strain energy density control volume for a nanoscale singular stress field, Fatigue Fract. Eng. Mater. Struct., 39(12) (2016) 1557–1564.
[138] Razavi, S.M.J., Ferro, P., Berto, F., Fatigue assessment of Ti–6Al–4V circular notched specimens produced by selective laser melting, Metals, 7(8) (2017) 291.
[139] Fergani, O., Berto, F., Welo, T., Liang, S.Y., Analytical modelling of residual stress in additive manufacturing, Fatigue Fract. Eng. Mater. Struct., 40(6) (2017) 971-978.
[140] Razavi, S.M.J., Ferro, P., Berto, F., Torgersen, J., Fatigue strength of blunt V-notched specimens produced by selective laser melting of Ti-6Al-4V, Theor. Appl. Fract. Mech., in press. DOI: 10.1016/j.tafmec.2017.06.021.
[141] Torgersen, J., Qin, X.H., Li, Z., Ovsianikov, A., Liska, R., Stampfl, J., Hydrogels for Two-Photon Polymerization: A Toolbox for Mimicking the Extracellular Matrix, Adv. Func. Mater., 23(36) (2013) 4542-4554.
[142] Li, Z., Pucher, N., Cicha, K., Torgersen, J., Ligon, S., Ajami, A., Husinsky, W., Rosspeintner, A., Vauthey, E., Naumov, S., Scherzer, T., Stampfl, J., Liska, R., A straightforward synthesis and structure–activity relationship of highly efficient initiators for two-photon polymerization, Macromolecules, 46(2) (2013) 352-361.

[143] Torgersen, J., Ovsianikov, A., Mironov, V., Pucher, N., Qin, X., Li, Z., Cicha, K., Machacek, T., Liska, R., Jantsch, V., Stampfl, J., Photo-sensitive hydrogels for three-dimensional laser microfabrication in the presence of whole organisms, J. Biomed. Opt., 17(10) (2012) 105008-105008.

[144] Coelho, R.S., Kostka, A., dos Santos, J.F., Pyzalla, A.R., Friction-stir dissimilar welding of aluminium alloy to high strength steels: Mechanical properties and their relation to microstructure, Mater. Sci. Eng. A 556 (2012) 175–183.

[145] Das, H., Basak, S., Das, G., Influence of energy induced from processing parameters on the mechanical properties of friction stir welded lap joint of aluminum to coated steel sheet, Int. J. Adv. Manuf. Technol., 64 (2013) 1653–1661.

[146] Ulf Roar Aakenes Industrializing of the Hybrid Metal Extrusion & Bonding (HYB) method – from prototype towards commercial process. (2013).

[147] Abbatinali, F., Characterization of AA6082-T6 Aluminium Alloy and S355 Steel Welding Achieved with the Hybrid Metal Extrusion & Bonding (HYB) Process, (2017).